

**Inhomogeneous Solvation Structure of I^- and
 Na^+ on the Surface of NaI Aqueous Solution**

(NaI水溶液表面における I^- と Na^+ の不均一な
溶媒和構造)

Department of Basic Science,
Graduate School of Arts and Sciences,
The University of Tokyo

Makoto Shoji

東海林 真

March 2012

Contents

Chapter 1	General Introduction	1
1.1	View of the Solution Surface of Electrolyte	1
1.1.1	Conventional View	1
1.1.2	New Picture from Laboratory Measurement	3
1.2	Surface Specific Researches	6
1.2.1	Theoretical Simulation	6
1.2.2	Vibrational Sum Frequency Generation Spectroscopy	9
1.2.3	Second Harmonic Generation Spectroscopy	10
1.2.4	Photoelectron Spectroscopy	11
1.3	Purpose of this Research	13
Chapter 2	Experimental Section	14
2.1	Overview of the Experiment	14
2.2	Liquid Beam	14
2.2.1	Method of Preparation	15
2.2.2	Supercooling of Liquid Beam Surface	16
2.2.3	Temperature of Liquid Beam Surface	16
2.2.4	Beam Diameter and Profile	18
2.3	Mechanism of Electron and Cation Ejection	21
2.3.1	Electron Ejection from Liquid Beam	21
2.3.2	Cation Ejection from Liquid Beam	22
2.4	Photodetachment Spectroscopy and Mass Spectrometry	23
2.4.1	Experimental Apparatus	23
2.4.2	Photodetachment Spectroscopy	25
2.4.3	Mass Spectrometry	26

Chapter 3 Solvation Structures of I⁻ and Na⁺ on and below a Surface of Aqueous Solution Studied by Photodetachment Spectroscopy and Mass Spectrometry	29
3.1 Introduction	29
3.2 Results and Discussion	30
3.2.1 Experimental Results.....	30
3.2.2 Photodetachment from I ⁻ on Aqueous Solution Surface	36
3.2.3 Solvation Structure of I ⁻ on Aqueous NaI Solution Surface	38
3.2.4 Solvation Structure of Na ⁺ on Aqueous Solution Surface Studied by Action Spectrum.....	39
3.2.5 Mass Spectrometric Study of the Solvation Structure of Na ⁺ on Aqueous Solution Surface	40
Chapter 4 Solvation Structure of I⁻ on a Surface of a Mixture Solution of KI and NaCl	45
4.1 Introduction	45
4.2 Results and Discussion	45
4.2.1 Solvation Structure of I ⁻ on Aqueous KI Solution Surface	45
4.2.2 Enhanced Surface I ⁻ Concentration by Addition of NaCl	47
Chapter 5 Conclusion	53
References	55
Appendix	58
Acknowledgements	74

Chapter 1

General Introduction

1.1 View of the Solution Surface of Electrolyte

1.1.1 Conventional View

Gas-liquid interfaces are ubiquitous in nature, and play an important role in physical, chemical, atmospheric, and biological processes.

Hence, researches on electrolyte solution surfaces flourished in the first half of the 20th century, following macroscopic measurements such as surface tension and surface potential.^[1-3] In particular, the surface of aqueous solutions containing salt was focused on because it was observed that surface tension increases upon addition of a salt to water. The Gibbs adsorption isotherm that gives the relationship between surface tension and surface excess is expressed as below.

$$\Gamma = -\frac{a}{RT} \left(\frac{\partial \gamma}{\partial a} \right)_T \quad (1)$$

Here Γ is the surface excess of the solute per unit area, a is the solute activity, R is gas constant, T is absolute temperature, γ is surface tension. $\left(\frac{\partial \gamma}{\partial a} \right)_T$ can be positive or negative value, which corresponds to negative adsorption and positive adsorption respectively. According to this equation, the result indicates the negative adsorption in the surface region. As a result, the idea that ions hardly exist on the surface region of electrolytes aqueous solution was commonly supported. This notion of ion-free surface

has been the conventional view.

Incidentally, Weissenborn measured the surface tension of aqueous solutions of simple inorganic, electrolytes (36 in total) by the maximum bubble pressure method as a function of electrolyte concentration up to 1 M in 1996.^[4] Table in the following shows the part of their result. The $\frac{d(\Delta\gamma)}{dc}$ corresponds to $\left(\frac{\partial\gamma}{\partial a}\right)_T$. It is found that the values of electrolytes aqueous solution are positive.

Electrolyte	$\frac{d(\Delta\gamma)}{dc}$
NaCl	2.08 ± 0.08
KCl	1.85 ± 0.05
NaI	1.23 ± 0.06
NaBr	1.83 ± 0.05
NaF	1.83 ± 0.06

1.1.2 New Picture from Laboratory Measurement

In the 1990s there was a renewed interest in the surfaces of electrolytes. Several research groups of atmospheric chemistry suggested that halogen anions must sit on the liquid surface as this would explain the mechanism of the chemical reactions observed in their experiments.^[5,6]

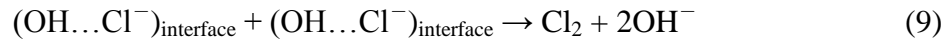
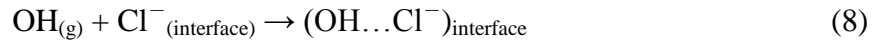
Hu et al. made the first suggestions that heavier halide anions reside at the air-water interface.^[5] They studied the uptake of molecular halogens X_2 ($X = \text{Cl}$ or Br) by droplets of aqueous NaY ($Y = \text{Br}$ or I) solutions, which was triggered primarily to the reaction $X_2 + Y^- \rightarrow \text{XY} + X^-$. The magnitude and concentration dependence of the measured uptake could not be described by a bulk phase reaction mechanism, and hence, Hu et al. suggested that reaction involving Y^- on the surface of the droplets should play a significant role in the uptake process.

Finlayson-Pitts and co-workers applied a combination of experimental, molecular dynamics, and kinetics modeling studies to a system of concentrated aqueous sodium chloride particles suspended in air at room temperature with ozone.^[6] In experimental study, they measured Cl_2 production in a chamber after 254 nm laser irradiation. O_3 is photolyzed by 254 nm irradiation and generates OH radicals in the gas phase, which can be taken up into the particles. OH is known to react in solution with Cl^- , generating Cl_2 as shown below.



Cl_2 production was calculated based on a kinetic model to evaluate mechanisms of Cl_2

formation in the experimental system. As a result, Cl_2 production measured experimentally are much larger than those predicted in the kinetic model. This means that conventional chemical and physical processes involving transport of gases to the particle surface, mass accommodation, diffusion, and known reactions in the bulk aqueous-phase of the particles, are not able to explain the experimental observations. They proposed that the key step in the generation of Cl_2 in the chamber is the reaction of OH with chloride at the interface as following.



This reaction scheme is not consistent with the conventional view that ions hardly exist on the surface region of electrolytes aqueous solution.

Figure 1.1 shows schematically the conventional reaction in the bulk aqueous phase of the particles and the newly proposed reaction at the gas/aqueous interface. In order to know the reaction processes, it is important to elucidate the solvation structure on the surface of aqueous solution.

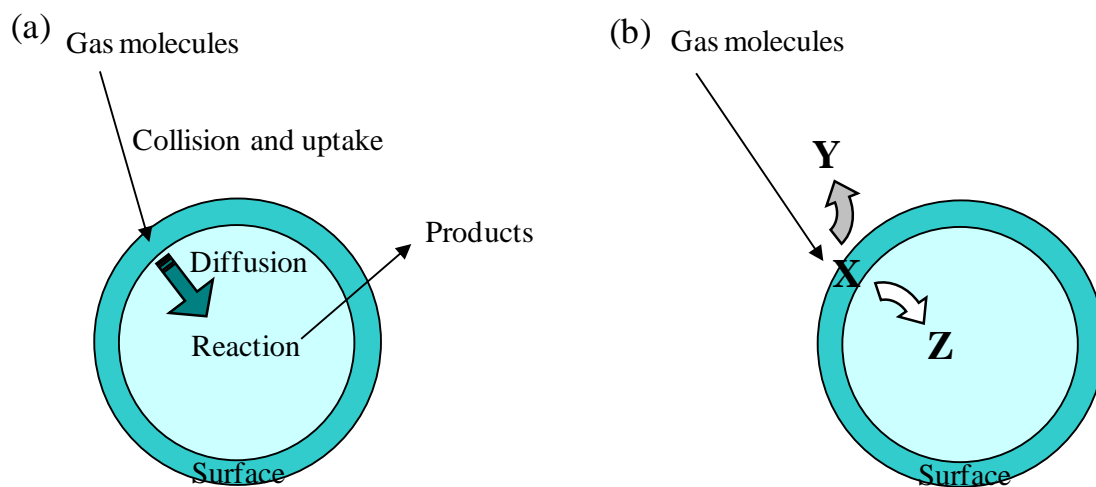


Figure 1.1: Schematic diagram of the reaction between gas molecules and droplet particle.

(a) Conventional known reaction (b) Newly proposed reaction (Gas molecules react with X on aqueous surface. Product Y is released into the gas phase and reactant Z diffuses into the bulk.)

1.2 Surface Specific Researches

Ion specificity at the air/water interface came into focus in order to rationalize the experimental results. Several research groups started surface specific researches as described below.

1.2.1 Theoretical Simulation

Jungwirth and Tobias modeled the air/solution interface by performing molecular dynamics (MD) simulations using polarizable potentials of water slabs containing sodium halide (fluoride, chloride, bromide, or iodide).^[7-10] Figure 1.2 shows typical snapshots and the density profiles within the slab of the ionic species and water oxygen atoms, obtained from the simulations.^[8] In the NaF solution, both ions are strongly repelled from the surface, leaving an ion-free 3.5 Å thick layer. This is in accord with the conventional view, in which ions are repelled from the air/water interface. In contrast, Cl⁻ and especially Br⁻ and I⁻ occupy a significant portion of the air/water interface. Quantitatively, this effect is illustrated by the density profiles in Figure 1.2.

They suggested that the propensity of large, polarizable anions locating at the interface can be explained qualitatively in terms of anisotropic solvation, which induces a substantial dipole on the ion. Figure 1.3 schematically shows a polarizable atomic anion in the aqueous bulk and at the air/water interface.^[10] In the liquid bulk, water molecules arrange roughly symmetrically around the ion. As a result, the vectorial sum of the dipoles of these water molecules is very small (zero on average). The situation is very different at the interface, where, schematically, water molecules are present only on one side of the ion. Consequently, there is a significant electric field resulting from the sum of water dipoles polarizing the anion. The resulting favorable dipole-induced dipole interactions compensate the loss of ion-dipole interactions, and hence, a large halide ion is able to transfer from the bulk solution to the interface.

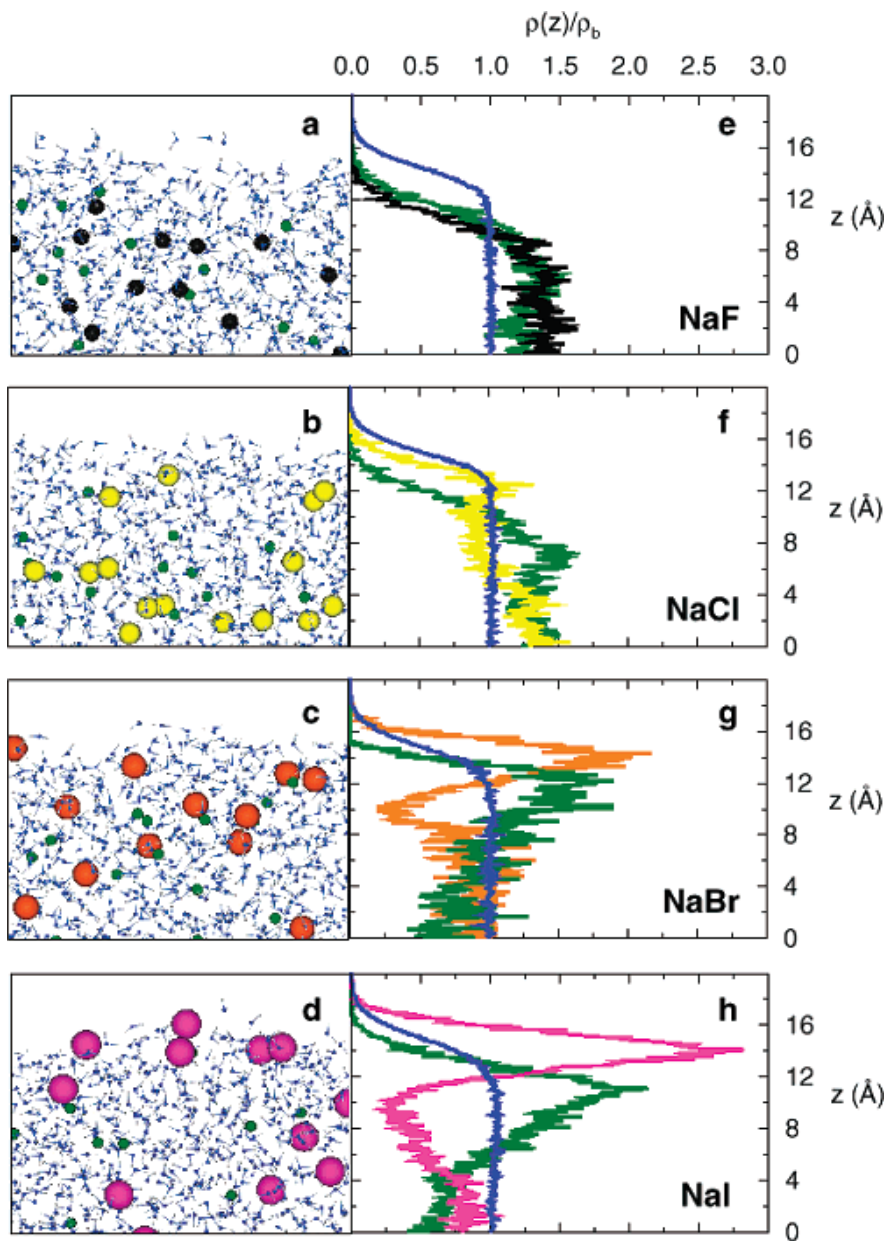


Figure 1.2: Molecular dynamics simulations of solution/air interfaces of solutions of sodium halides. **(a-d)** Snapshots of Na^+ (small green balls) and the halide ions (black = F^- ; yellow = Cl^- ; orange = Br^- ; pink = I^-). **(e-h)** Profiles for O, Na, and the halide ions from the center of the water slab ($z = 0$) to the air-water interface and beyond.^[10]

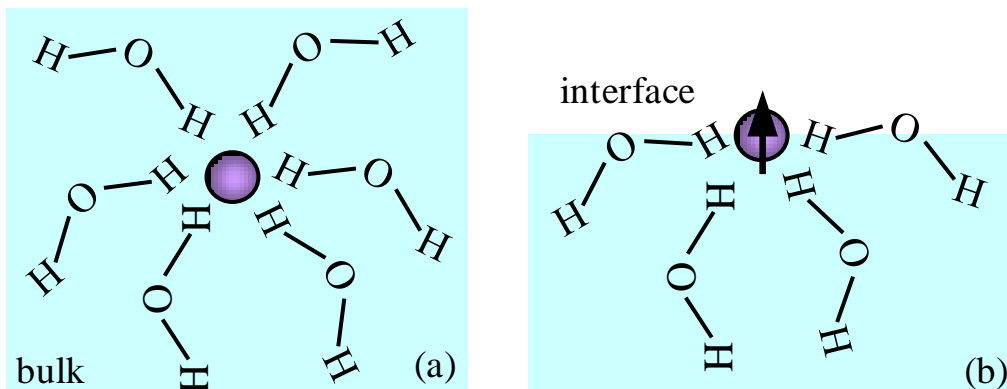


Figure 1.3: A schematic picture of interactions between a polarizable anion and water molecules (a) in the aqueous bulk, and (b) at the air/water interface.

1.2.2 Vibrational Sum Frequency Generation Spectroscopy

Surface enhancement of polarizable anions proposed above has been investigated experimentally. Vibrational sum frequency generation (SFG) spectroscopy is one of the interface-selective experimental techniques. SFG is a second-order nonlinear optical process in which two input laser beams at frequencies ω_{IR} and ω_{V} , which correspond to frequencies of the infrared and the visible respectively, overlap in a medium and generate an output at the sum frequency $\omega_{\text{S}} = \omega_{\text{IR}} + \omega_{\text{V}}$ (see Figure 1.4). A second-order process is forbidden in media with centrosymmetry in the electric dipole approximation but selectively allowed in noncentrosymmetric environments such as surfaces or interfaces.^[11] Therefore the process is highly surface-specific. When ω_{IR} , ω_{V} , or ω_{S} approaches a surface resonance, the SFG output is resonantly enhanced. This provides vibrational spectra of molecules at the interface.

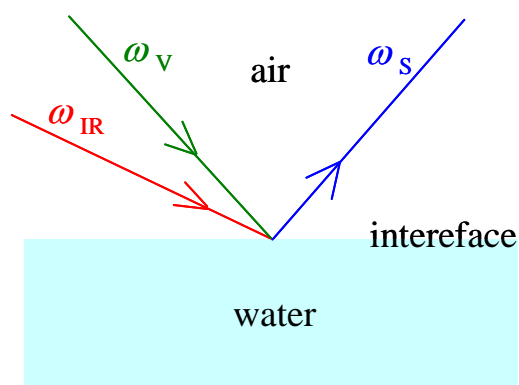


Figure 1.4: Geometry for sum frequency generation from air/water interface.

Allen and co-workers studied air-aqueous sodium halide (NaF, NaCl, NaBr and NaI) interfaces using vibrational SFG spectroscopy, and Raman and IR spectroscopies were also used to compare the effects of halide anions on water structure of the bulk solution to that of the interface.^[12] They concluded that comparison of the surface spectra to the bulk spectra indicates the higher concentrations of Br^- and I^- in the interfacial region relative to the bulk, because a peak area ratio providing the information about the hydrogen bonding perturbed by ambient anions in SFG spectra is greater than the Raman \times IR (Raman area multiplied by ATR-FTIR area) ratios.

In contrast, Richmond and co-workers gave different view on the surface region of aqueous sodium halide solutions.^[13] They concluded that there are few ions in the topmost surface layer of the surface region because the uncoupled donor OH that

resides in the topmost portion of the surface region does not exhibit significant spectral changes for any solutions unlike bulk studies.

The disagreement in the interpretation of the SFG spectra arises from the difficulty in interpretation due to indirect technique that observes water structure influenced by ambient ions.

1.2.3 Second Harmonic Generation Spectroscopy

Second harmonic generation (SHG) spectroscopy is also one of the interface-selective experimental methods. SHG is a second-order nonlinear optical process, similar to SFG, in which an input laser beam at a frequency, ω , generates an output at frequency, 2ω . The SHG response is expressed in terms of the second-order susceptibility.^[14]

$$I_{2\omega} \propto |\chi^{(2)}|^2 \times I_{\omega}^2 \quad (10)$$

$$\chi^{(2)} = \chi_{\text{water}}^{(2)} + \chi_{\text{iodide}}^{(2)} \quad (11)$$

$$\chi_{\text{iodide}}^{(2)} = N_S \times \langle \beta \rangle \quad (12)$$

Here, I_{ω} and $I_{2\omega}$ are the fundamental and the SHG intensity, respectively, $\chi^{(2)}$ is the second-order susceptibility, N_S is the number of molecules probed at the surface, and $\langle \beta \rangle$ is the molecular second-order susceptibility. When either the fundamental or the SHG wavelength are resonant with a molecular/atomic transition, the non-linear susceptibilities are greatly enhanced.

Saykally and co-workers studied interfacial structure of aqueous electrolytes with femtosecond SHG spectroscopy.^[14-16] They measured SHG intensity of dilute sodium iodide solution at the air/water interface as a function of the wavelength of an input laser. The Gibbs excess energy of adsorption was calculated from formula 10, 11 and 12, and

Langmuir isotherm given below.

$$N_s = \frac{N_s^{\max} \times x}{x + 55.5 \text{ mol/l} \times \exp(\Delta G_{\text{Ads}}/RT)} \quad (13)$$

Here, N_s^{\max} is the saturated surface concentration, x is the bulk concentration and ΔG_{Ads} is the Gibbs excess free energy of adsorption. They calculated ΔG_{Ads} of iodide anions at the air/water interface of -6.1 ± 0.2 kcal/mol, which indicates an enhanced surface concentration of iodide anions in dilute solution.

SHG spectroscopy is the direct technique compared to SFG spectroscopy, but it has difficulty that SHG intensity is much weaker by a factor of about 10^{10} than the fundamental.

1.2.4 Photoelectron Spectroscopy

In addition to nonlinear spectroscopic technique, photoelectron spectroscopy has been employed as the surface specific technique. Faubel et al. obtained photoemission spectra from aqueous sodium iodide solutions using a liquid microjet and EUV synchrotron radiation.^[17] A detail of the liquid microjet method is shown in the next chapter because it is also used in our experiment. This technique enables the observation of electron emission from the surface area of sodium iodide solutions. Measuring the photoelectron intensity as a function of the bulk concentration, they found identical behavior for sodium and iodide ions, and concluded negative surface excess for NaI which contradict the predictions of MD simulations.^[7-9] But they also say that the surface sensitivity of their experiment, a few molecular layers, is insufficient to resolve density profile changes within a region being small compared to the electron information depth.

Salmeron et al. investigated the ion composition in the surface region of KBr and KI aqueous solutions by applying x-ray photoelectron spectroscopy (XPS) to salt crystals

~2 mm thick and ~5 mm² mounted on a cooled copper substrate in contact with water vapor.^[18] They studied an alkali-halide sample as a function of water vapor pressure, starting with the freshly cleaved, dry sample up to the deliquescence point of the salts using the recent development of techniques to acquire photoemission spectra in gas environments at pressures up to several torr.^[19] In their experiments, the K 2p and 3p, the O 1s, and the C 1s peaks were monitored, as well as the Br 3d and I 4d peaks for KBr and KI, respectively. They measured relative anion/cation signals for identical photoelectron kinetic energies (KEs). The use of the same KE ensures that the sample depth analyzed is the same for all of the elements. Figure 1.5 demonstrated that the anion concentrations were enhanced relative to the cation concentrations in the interfacial region, and this trend is more remarkable for iodide than bromide. The results appeared to be consistent with the qualitative predictions by the MD simulations.

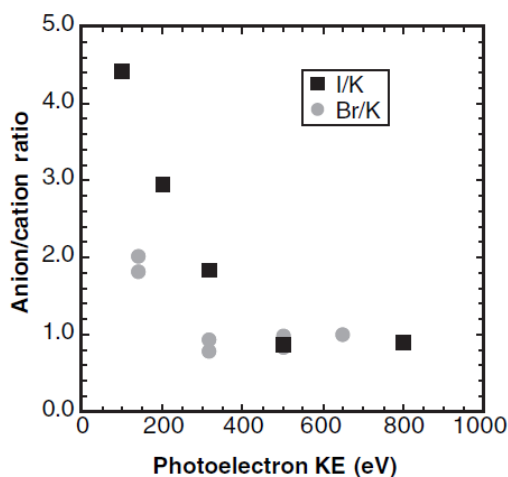


Figure 1.5: Measured anion/cation atomic ratio as a function of the photoelectron kinetic energy. The circles are the measured Br/K ratios for KBr. The squares are the values of I/K for KI.

1.3 Purpose of this Research

As mentioned in the previous section, the researches containing simulations and experiments about electrolyte solution surface have been conducted by many groups. Some of the results suggest surface enhancement of anions, that rationalizes the results of the atmospheric research groups. However, this picture is still not perfect, as some disagreements in the interpretation exist, because of the difficulties of probing the liquid surface. For example, SFG spectroscopy is indirect technique in that it observes not electrolyte ion itself but water structure influenced by ambient ions, and SHG spectroscopy has difficulty that SHG intensity is much weaker than the fundamental. Especially, solvation structures of cations are hardly determined by these experimental methods. Anyway, highly sensitive technique for overcoming the difficulty is needed to probe the liquid surface.

The purpose of the present research is to investigate solvation structures of I^- and Na^+ on a NaI aqueous solution surface using a liquid beam by photodetachment spectroscopy and time-of-flight (TOF) mass spectrometry. Liquid beam method is established as a tool probing the liquid surface. Photodetachment spectroscopy and TOF mass spectrometry are highly sensitive tools in studies of molecules isolated in the gas phase. We combined these technique and observed electrons and ions emitted from the liquid beam of NaI aqueous solution upon irradiation of the liquid beam with a UV laser pulse. The detail of the experimental technique will be explained in the next chapter.

In addition, we extended this research to the solvation structure of I^- on a surface of a mixture aqueous solution of KI and NaCl in order to elucidate the influence of the other ions.

Chapter 2

Experimental Section

2.1 Overview of the Experiment

As mentioned in section 1.3, we conducted two types of experiments in the present study. One is photodetachment spectroscopy and the other is TOF mass spectrometry. Both are combined with liquid beam technique, and the electrons are observed in the former, while the cations are observed in the latter. The electrons and the cations are emitted from a liquid beam of a NaI aqueous solution upon irradiation with a UV laser pulse onto a liquid beam introduced into a vacuum. The detail of the experimental technique will be explained in the following.

2.2 Liquid Beam

We utilized a liquid beam method as the experiment probing liquid surface. A liquid beam has been developed by Faubel et al as a technique for introducing a continuous thin liquid flow into a vacuum.^[20] Cleanliness of the liquid beam surface is maintained even at a pressure of 10^{-5} – 10^{-6} Torr because a reasonably high-speed flow always renews the liquid beam surface. In this section, the instrumentation of a liquid beam is described in detail.

2.2.1 Method of Preparation

Figure 2.1 is the nozzle we used for forming a liquid as a thin beam. The thin nozzle plate is made of platinum and has an aperture of 20 μm in diameter, which was soldered onto the end of a 45 mm stainless steel tube. This aperture plate is diverted from a commercial platinum aperture used in an electron microscope. When a Shimadzu LC-10Ai pump designed for a liquid chromatography supplies this nozzle with the continuous liquid flow at a flow rate of 0.2 ml min^{-1} , a stable continuous liquid beam is ejected through an aperture plate.

In order to obtain a liquid as a thin beam, the Reynolds number of the flow, R_e , has to be in a suitable range ($100 < R_e < 1000$), which satisfies the laminar flow condition.^[23] At lower values of R_e , the liquid flow becomes unstable and forms a single droplet at the aperture exit, whereas at higher R_e the droplet disintegrates immediately on leaving the nozzle. In the present study, we can make a stable liquid beam by keeping a flow rate at 0.2 ml min^{-1} .

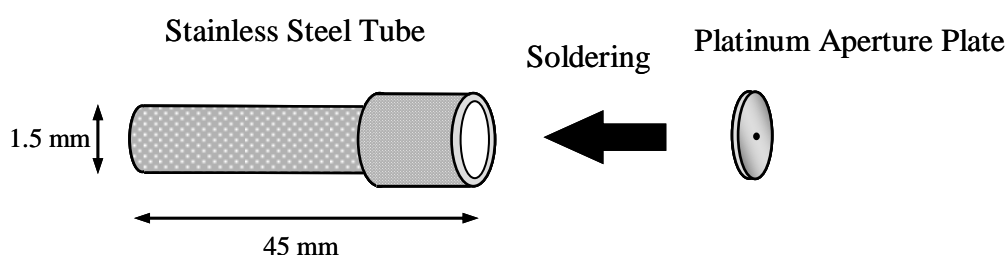


Figure 2.1: A liquid beam nozzle for emitting a liquid as a thin beam. Platinum plate has an aperture of 20 μm in diameter.

2.2.2 Supercooling of Liquid Beam Surface

Liquid beam is introduced into vacuum chamber as shown in Figure 2.2. However, difficulty arises in the preparation of a water liquid beam; the liquid beam surface is supercooled because of evaporative cooling, and as a result, the liquid beam itself tends to form ice on reaching the surface of the cryopump. An ice stick grows from the cryopump surface toward the nozzle and clogs the nozzle aperture. In order to resolve this problem, a chopper is mounted just above the cryopump surface to avoid this icing by slicing the liquid beam.

2.2.3 Temperature of Liquid Beam Surface

The evaporative cooling mentioned in the previous section causes a temperature drop on the liquid beam surface with distance from the nozzle exit. Faubel et al estimated the temperature of a water liquid beam from the measured velocity distribution of molecules vaporizing from the liquid beam surface, on the assumption that the surface is in equilibrium with the evaporating molecules.^[21] The temperature is found to drop by ~30 K at 4 mm downstream from the nozzle, whereas the liquid beam remains liquid within a distance of several millimeters to centimeters from the nozzle, as proved by the lack of substantial scattering of the laser beam due to either Rayleigh instabilities or a liquid-solid phase transition when the laser is allowed to transmit inside the liquid beam, which behaves as a light guide.

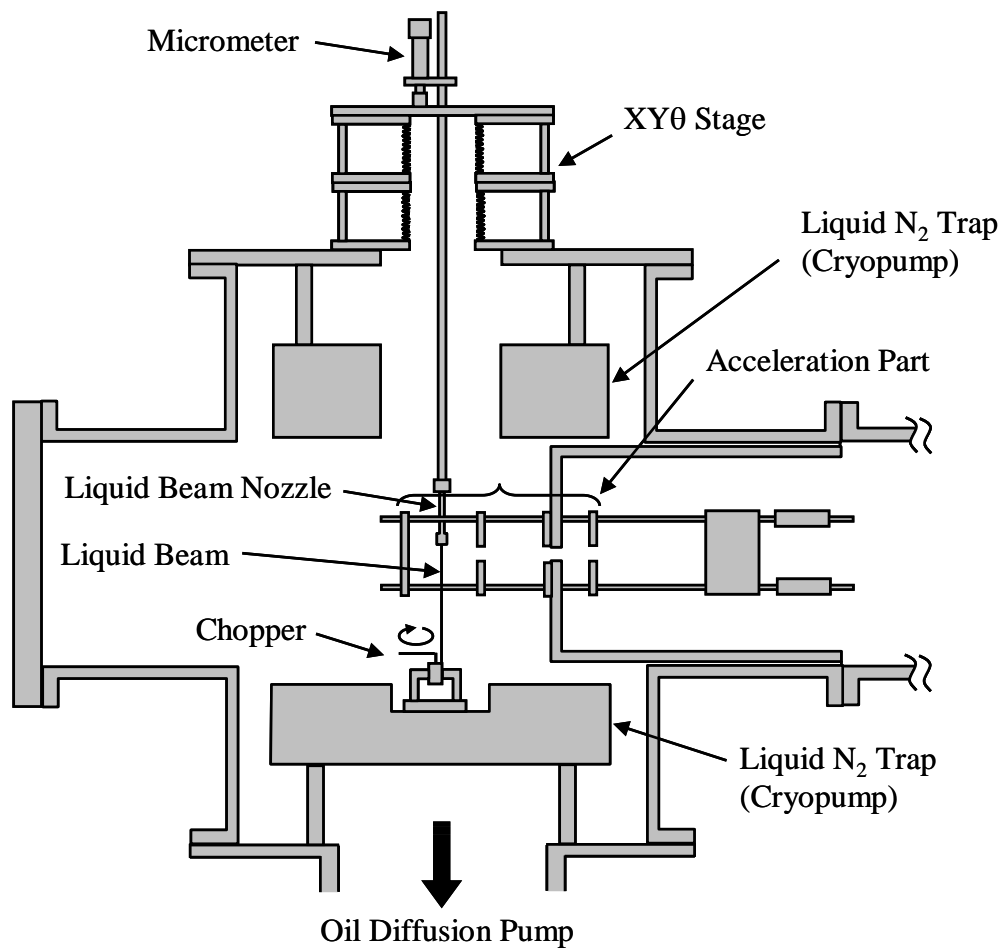


Figure 2.2: Schematic diagram of the experimental setup of the part introducing liquid beam into a vacuum vessel. The right blind part is composed mainly of detector and described containing acceleration part in the later section.

2.2.4 Beam Diameter and Profile

A liquid beam exhibits a clear optical diffraction pattern when it is illuminated by the laser perpendicularly to the liquid beam, since a liquid beam behaves like a stable liquid filament. We estimated the diameter of a liquid beam by observing an optical diffraction pattern as shown in Figure 2.3. Here, incident laser wavelength is 266 nm, the laser irradiation position of a liquid beam is at a distance of 1 mm from the aperture, and liquid beam sample is an aqueous solution of resorcinol which has a strong absorption in 266 nm.

Figure 2.4 shows a typical diffraction pattern, together with the intensity profile of experimental and theoretical, the latter is given by the Fraunhofer diffraction arising from the interference of light obstructed by the liquid beam.^[22]

The intensity profile is expressed by

$$I = \frac{I_0(\sin^2 \beta)}{\beta^2} \quad (14)$$

$$\beta = \frac{\pi b \sin \theta}{\lambda} \quad (15)$$

where I_0 is the intensity of the scattering light at the center, b is the diameter of the liquid beam, θ is the diffraction angle, and λ is the wavelength of the incident laser. From the fact that theoretical and experimental curves coincide strikingly, a liquid beam is regarded as a stable continuous liquid flow. The diameter of the liquid beam is determined to be 20.5 μm through analysis of the pattern and is essentially equal to the diameter of the nozzle aperture ($\sim 20 \mu\text{m}$).

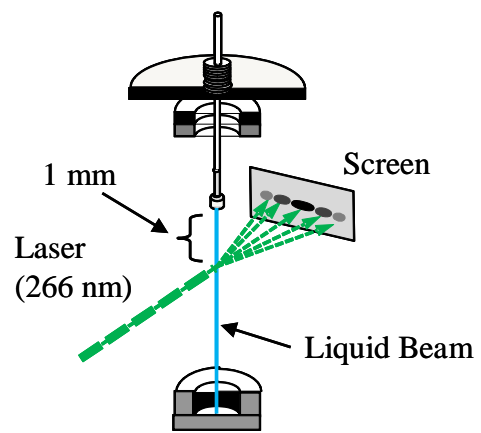


Figure 2.3: Schematic diagram of experimental apparatus investigating optical diffraction pattern by laser illumination perpendicular to the liquid beam.

We also observed the diffraction patterns changing the laser irradiation position of a liquid beam as shown in Figure 2.5. Clear diffraction patterns are obtained at a distance of less than 1.7 mm from the aperture, but the pattern becomes unclear after 1.7 mm. This indicates that a liquid beam maintains continuous liquid condition at a distance of less than 1.7 mm from the aperture.

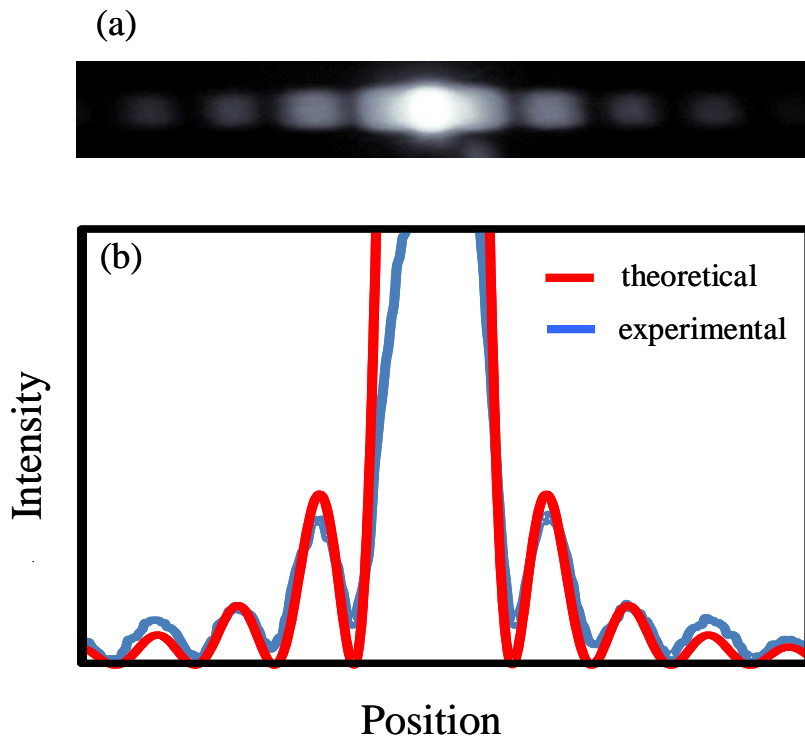


Figure 2.4: Optical diffraction pattern generated by illumination of an UV laser (266 nm) onto the liquid beam (a) and its intensity profile (b). (Red curve) The fitted curve is calculated on the basis of the Fraunhofer diffraction pattern arising from the interference of light obstructed by the liquid beam; (Blue curve) Experimental intensity profile.




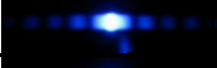
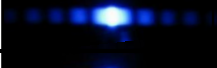
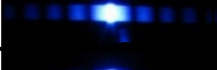
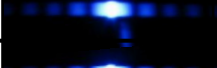
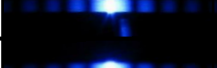
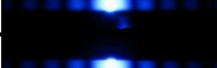
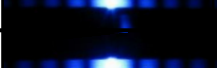
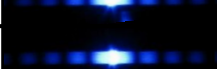
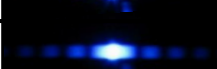
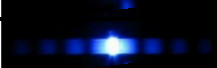
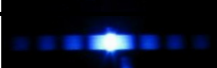
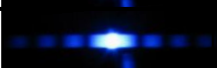
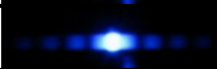
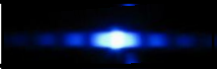



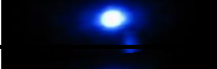

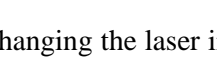
Distance (mm)	Pattern
0.1	
0.2	
0.3	
0.4	
0.5	
0.6	
0.7	
0.8	
0.9	
1.0	
1.1	
1.2	
1.3	
1.4	
1.5	
1.6	
1.7	
1.8	
1.9	
2.0	
2.2	
2.4	
3.0	

Figure 2.5: The diffraction patterns changing the laser irradiation position of a liquid beam. “Distance” represents the distance from the aperture.

2.3 Mechanism of Electron and Cation Ejection

The liquid beam introduced into a vacuum chamber was crossed with a pulsed UV laser. The wavelength of the laser used in the present study is 216–280 nm which is resonant to the excitation of I^- in water. After the irradiation of the laser, electrons and cations are ejected from the liquid beam surface of NaI aqueous solution. This ejection mechanism is described in this section.

2.3.1 Electron Ejection from Liquid Beam

Figure 2.6 is the absorption spectrum of NaI aqueous solution. The band in ~220 nm is called the charge-transfer-to-solvent (CTTS) band, which is identified as the electronic transition from the ground state to the first electronic excited state of I^- in the solutions.^[24] In the excited state, the valence electron of I^- is weakly bound to I. Hence, the weakly bound electron can be released as a solvated electron into the solutions in a picosecond timescale (~70 ps). On the solution surface, absorption of another photon either by the excited I^- or the solvated electron causes one electron to be liberated into the vacuum. The electron escape depth is limited, and this is described in detail in the next chapter. In contrast to the surface, an electron released in the bulk phase stays inside liquid. This two-photon ionization is the mechanism of the electrons ejection from the liquid beam surface.

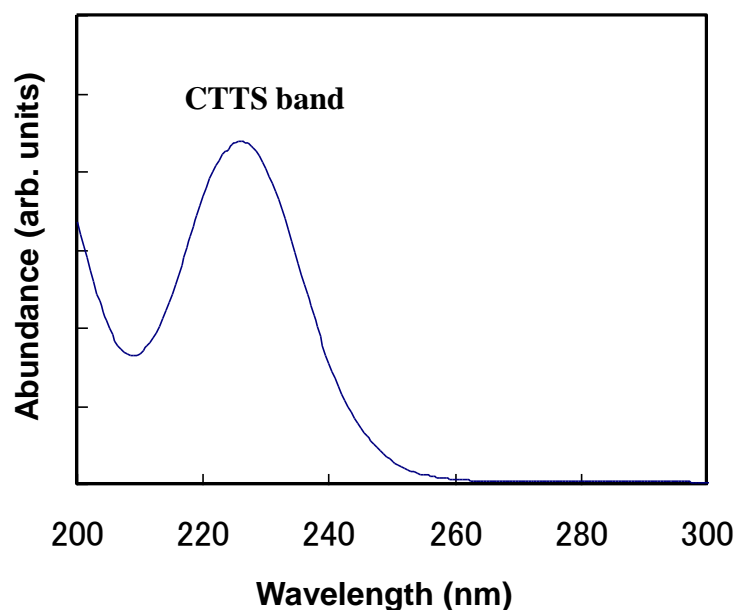


Figure 2.6: Absorption spectrum of NaI aqueous solution.

2.3.2 Cation Ejection from Liquid Beam

Under irradiation of the laser on the liquid beam, electrons generated by the photoionization escape from the surface region of the liquid beam, so that a surface region turns out to be positively charged because of electron depletion from the surface region. When a repulsive Coulomb force exerted toward a cation of interest from its neighboring cations exceeds the solvation energy of the cation, the cation is ejected exclusively from the surface (Coulomb ejection model). This model has been scrutinized by measurement of the intensities of the ions ejected into the gas phase and the ions remaining inside the liquid beam as a function of the ionization laser power by Kondow and co-workers.^[25]

2.4 Photodetachment Spectroscopy and Mass Spectrometry

2.4.1 Experimental Apparatus

Figure 2.7 shows schematic diagrams of the experimental apparatus used in the present study. Figure 2.7a and b exhibit setups for photodetachment spectroscopy and mass spectrometry, respectively. In both experiments, a liquid beam was introduced into a vacuum chamber through an aperture with a diameter of 20 μm . An aqueous solution of NaI was pressurized by a Shimadzu LC-10Ai pump designed for liquid chromatography, and a flow rate was maintained at 0.2 $\text{mL}\cdot\text{min}^{-1}$ to form the stable liquid beam in a vacuum. The liquid beam was trapped on a surface of a cryopump cooled by liquid N_2 at a distance 10 cm downstream from the aperture. A chamber of the liquid beam was evacuated down to 10^{-6} – 10^{-7} Torr by a 2400 L s^{-1} diffusion pump. Traveling a distance of 1 mm from the aperture, the liquid beam was crossed with a pulsed UV laser.

The pulsed UV laser (216–280 nm) was generated by frequency-doubling the output of a dye laser using BBO crystals. The wavelength of the laser was set to be resonant to the excitation of I^- in water. The pulse energy, which was monitored by Coherent FieldMax-P laser energy meter, was kept at 20–100 $\mu\text{J pulse}^{-1}$. The UV laser irradiated the liquid beam after passing through an optical lens with a focal length of 300 mm. The diameter of the liquid beam at the laser-irradiated position was almost the same as that of the aperture (20 μm). The beam waist of the excitation laser at the same position was about 0.1 mm, which is significantly larger than the diameter of the liquid beam.

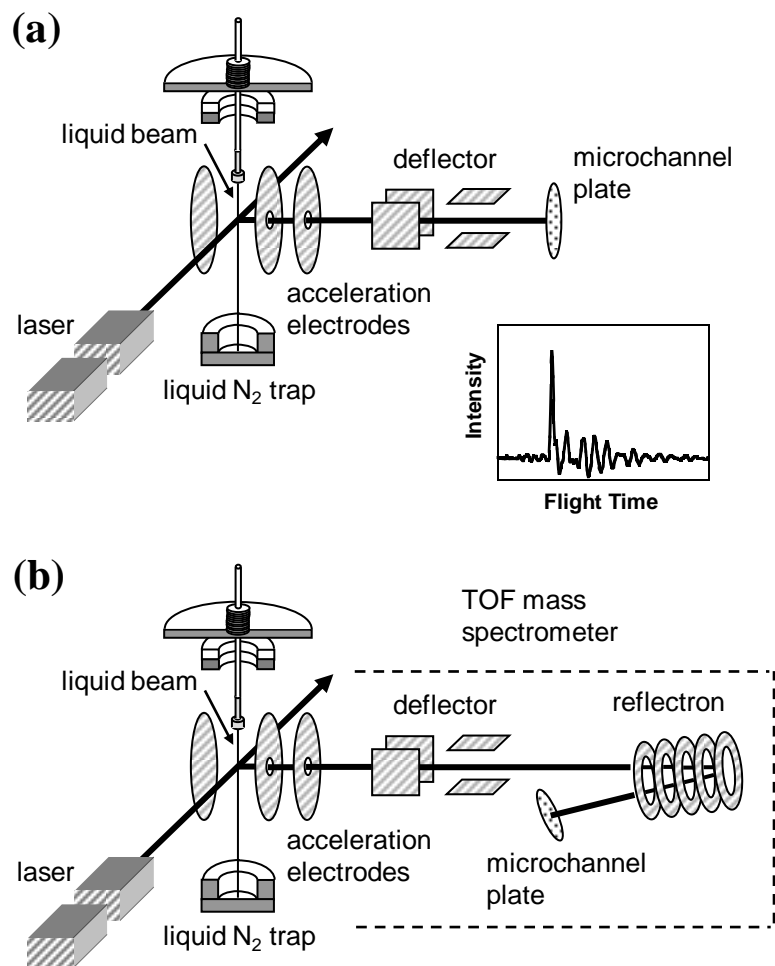


Figure 2.7: Schematic diagrams of experimental apparatus using a liquid beam for (a) photodetachment spectroscopy and (b) a TOF mass analysis. The inset in panel (a) exhibits a typical signal appearing in photodetachment spectroscopy.

2.4.2 Photodetachment Spectroscopy

In photodetachment spectroscopy and mass spectrometry, the same vacuum chamber is used. In this subsection, only outline of photodetachment spectroscopy is described. The detail of the experimental apparatus is explained in next subsection.

Photodetachment spectra were measured using the experimental setup shown in Figure 2.7a. Electrons ejected from the liquid beam into the vacuum were accelerated by a continuous electric field in the direction perpendicular to both the liquid and the laser beams. The electrons were guided by a set of vertical and horizontal deflectors. After traveling a 0.8 m field-free region, the electrons were detected by a Hamamatsu microchannel plate. The detector was placed away from the liquid beam and off-axis of the accelerated electron beam so that light scattered by the liquid beam could not reach the detector, since this would cause electrical noise on the detector. The abundance of the emitted electrons was measured as a function of excitation laser wavelength. Signals from the detector were amplified by a SRS SR445A preamplifier and processed by Tektronics TDS360P digital oscilloscope. The inset in Figure 2.7a exhibits the signal obtained in this setup.

2.4.3 Mass Spectrometry

Mass spectra of cations ejected from the liquid beam were obtained using a time-of-flight (TOF) mass analyzer as shown in Figure 2.7b. The cations ejected into the vacuum were accelerated by a pulsed high-voltage electric field applied in the first and second acceleration region for the TOF mass analysis. The cations were then steered by a set of vertical and horizontal deflectors. After traveling in a 1 m field-free region, the cations were reversed by the reflectron tilted by 3° off the beam axis and were detected by a Hamamatsu microchannel plate. Signals from the multiplier were amplified and processed using the same techniques used for the photodetachment spectroscopy. The mass resolution, $m/\Delta m$, was found to be more than 100 at $m = 200$ under the present experimental conditions. The detail of each part is described in the following.

Pumping Systems

The use of a liquid beam has the benefit of making the gas load for pumping low enough to maintain an ambient pressure of $\sim 10^{-5}$ Torr or less with moderately sized pumps (pumping speed $\sim 1200 \text{ Ls}^{-1}$), in combination with a cold trap, which serves as a cryopump. The cryopump has an effective pumping speed of 6000 Ls^{-1} for a condensable gas. A pressure of $\sim 10^{-5}$ Torr is sufficiently low to prevent ejected cluster ions from being perturbed during their travel to the detector. The flight tube for the mass analysis is differentially evacuated by a 3600 Ls^{-1} diffusion pump. An aperture with 3 mm in diameter, which is located in the entrance of the flight tube, serves as a conductance barrier, and the ambient pressure in the flight tube reaches 10^{-6} – 10^{-7} Torr.

Acceleration

Ions ejected from a liquid beam are accelerated by an electric field generated from four electrodes as shown in Figure 2.8. A pulsed electric field is applied in the primary acceleration region, with a certain delay time after the laser photoionization, and a constant electric field is applied in the secondary acceleration region. Adjusting the delay time and the electric field intensity ratio, E_d/E_s properly, one can attain a sufficient mass resolution measurement.

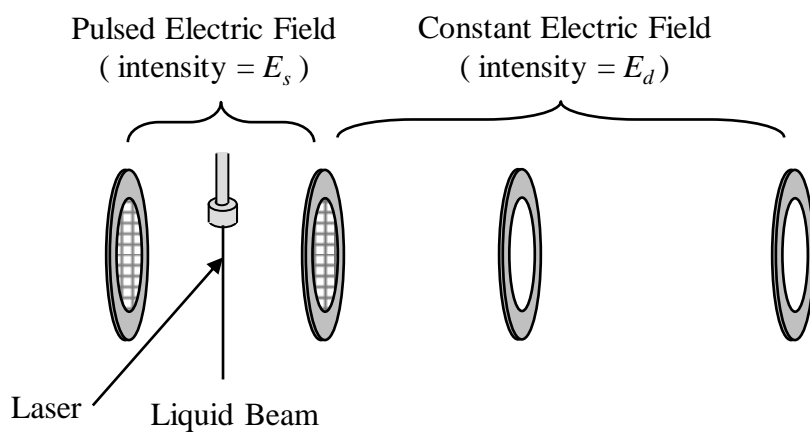


Figure 2.8: Acceleration Part consisted of four electrodes.

Reflectron

After passing through the acceleration region, the cations are then steered by a set of vertical and horizontal deflectors. After traveling in a 1 m field-free region, the cations were reversed by the reflectron tilted by 3° off the beam axis. Reflectron is consists of several electrodes, and a strong and a weak electric fields are applied in the each region as shown in Figure 2.9. Reflectron reduces the velocity spread of ions because the ion with larger kinetic energy travels the longer distance. Adjusting the voltage V_1 and V_2 properly, one can attain a high mass resolution measurement.

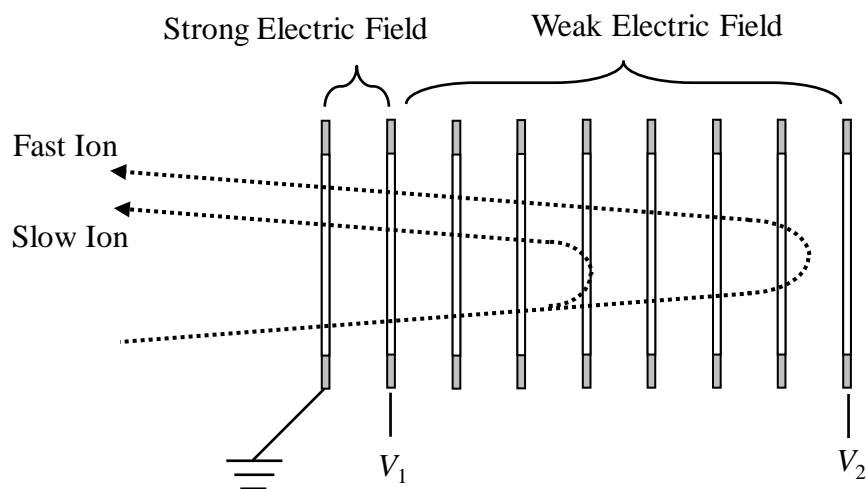


Figure 2.9: Reflectron consisted of several electrodes.

Chapter 3

Solvation Structures of I^- and Na^+ on and below a Surface of Aqueous Solution Studied by Photodetachment Spectroscopy and Mass Spectrometry

3.1 Introduction

In the present study, we investigated solvation structures of I^- and Na^+ on a NaI aqueous solution surface using a liquid beam by photodetachment spectroscopy and mass spectrometry. The use of the liquid beam in combination with photoelectron- and mass-spectroscopy is an established, high sensitivity technique for probing the properties of the liquid surface. We observed the electrons and the cations emitted from a liquid beam of NaI aqueous solution upon irradiation of the liquid beam with a UV laser pulse. We discussed electron escape depth from the solution surface based on the changes of spectral intensity as a function of the NaI concentration. In addition, it was found that we can selectively excite either I^- on the surface or I^- below the surface by tuning the wavelength of the UV laser. Based on this selectivity, the solvation structure of Na^+ on the aqueous solution surface was determined from the change in the mass spectra of the cations as a function of laser excitation wavelength.

3.2 Results and Discussion

3.2.1 Experimental Results

In the present experiment, we focused on the abundance of electrons emitted from the liquid beam, knowing that kinetic energies of the emitted electrons could relate to the binding energies of the electrons to the I atoms, which will be discussed in the later section. Figure 3.1 shows the abundance of the electrons as a function of the pulse energy of the excitation laser at 220 nm. The abundance increases with an increase in the pulse energy. The order of increase was estimated to be 1.2 ± 0.1 .

Figure 3.2 shows the abundance of electrons as a function of the wavelength of the excitation laser (photodetachment spectra) for 0.5, 1.0, 1.5, and 2.0 M NaI aqueous solutions. Overlaid on each of the photodetachment spectra is the absorption spectrum of aqueous NaI (solid line). It is well established that this broad absorption feature is the charge-transfer-to-solvent (CTTS) band of I^- . At 0.5 M, the photodetachment spectrum shows essentially a single peak at 225 nm, which is almost the same as the CTTS band of I^- in the solution. As the NaI concentration is increased, a second peak begins to appear at longer wavelengths than the CTTS band of I^- in the solution. To understand this concentration dependence, the abundance of the electrons was measured as a function of the NaI concentration at fixed wavelengths of the excitation laser (see Figure 3.3). The abundance of electrons does not change so much at 220 nm and increases at 240 nm with the NaI concentration.

To analyze solvation structures of Na^+ on the NaI aqueous solution surface, we measured the mass spectrum of cations ejected from the liquid beam surface. Figure 3.4 shows a typical mass spectrum of the cations produced from the liquid beam of the 0.5 M NaI aqueous solution, when the liquid beam was excited at 260 nm. The ions assignable to $Na^+(H_2O)_m$ ($m = 0, 1, 2, \dots$), appear in the mass spectrum. Figure 3.5 panels a and b show the total abundance of the cations as a function of the wavelength of the excitation laser (action spectrum) for the 0.5 and 1.5 M NaI aqueous solutions,

respectively. The action spectrum of the 0.5 M NaI aqueous solution is similar to the photodetachment spectrum of the 0.5 M NaI aqueous solution, showing the single broad band of I^- at 225 nm. The action spectrum of the 1.5 M NaI aqueous solution however, did not show the peak at longer wavelengths that was evident in the photodetachment spectrum of the same solution.

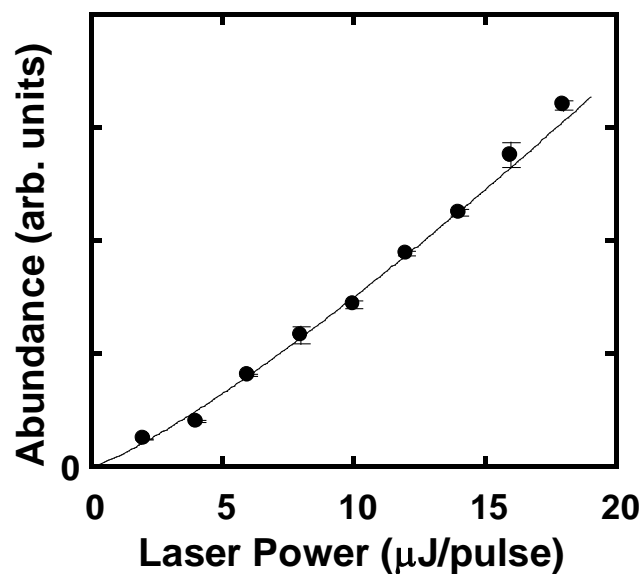


Figure 3.1: The abundance of electrons as a function of the pulse energy of the excitation laser at the wavelength of 220 nm.

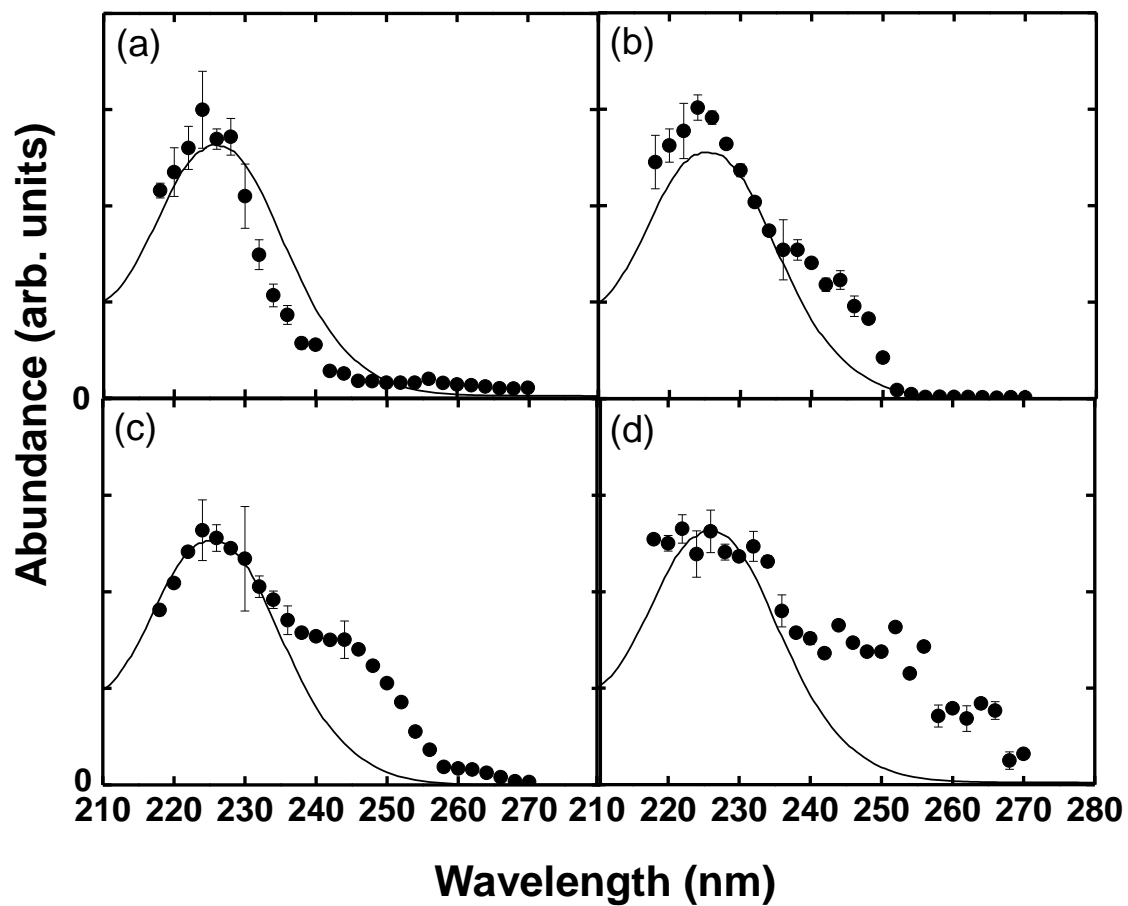


Figure 3.2: Photodetachment spectra which represent the abundances of the electrons as a function of the wavelength of the excitation laser for (a) 0.5, (b) 1.0, (c) 1.5 and (d) 2.0 M NaI aqueous solution.

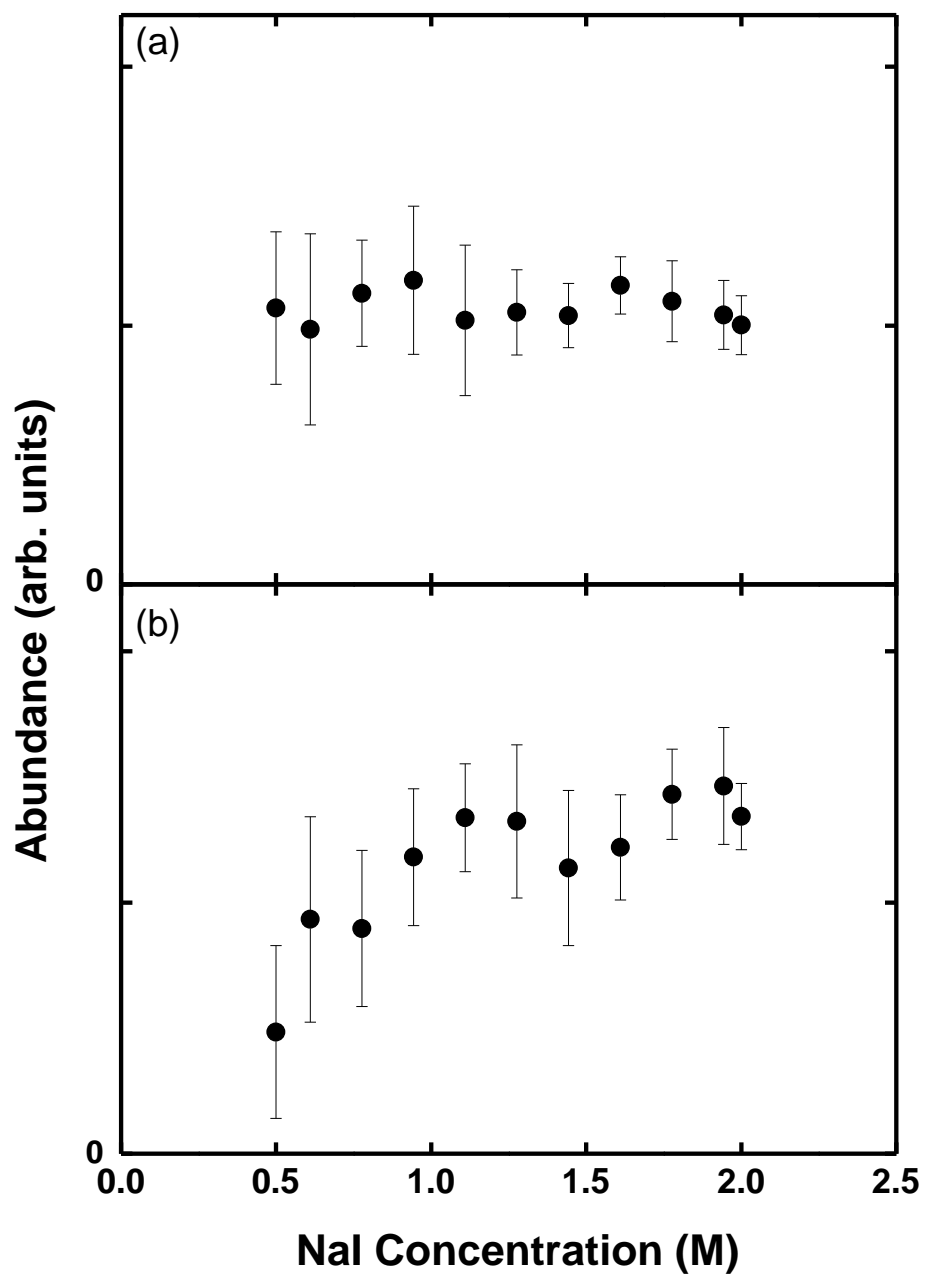


Figure 3.3: The abundances of the electrons as a function of the NaI concentration at fixed wavelengths of the excitation laser at (a) 220 and (b) 240 nm.

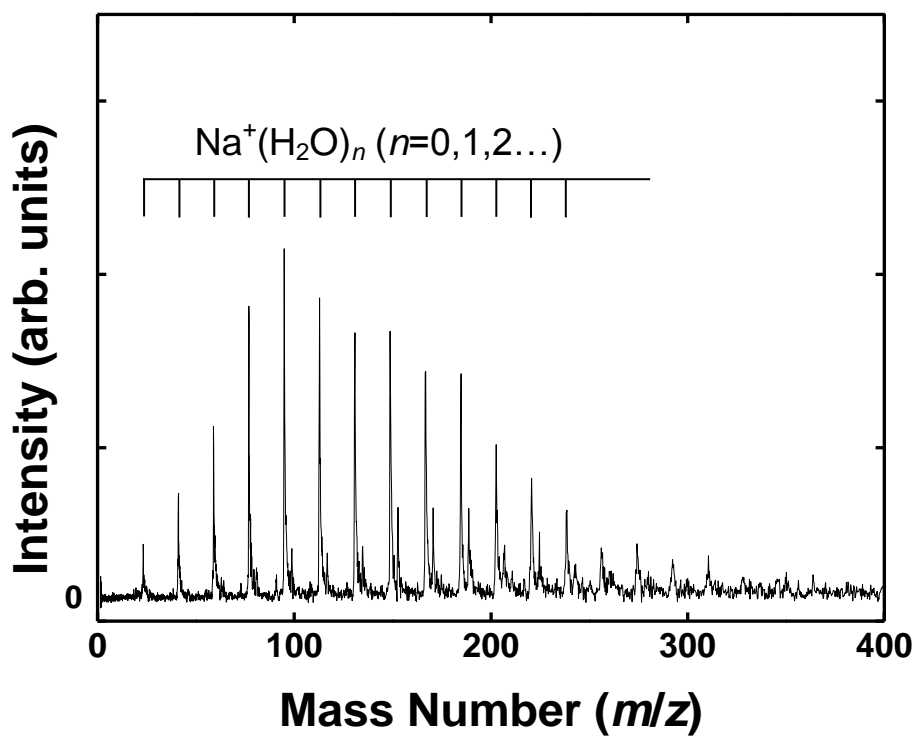


Figure 3.4: TOF mass spectrum of cations produced by irradiation of a 260 nm laser pulse onto the liquid beam of the 0.5 M NaI aqueous solution.

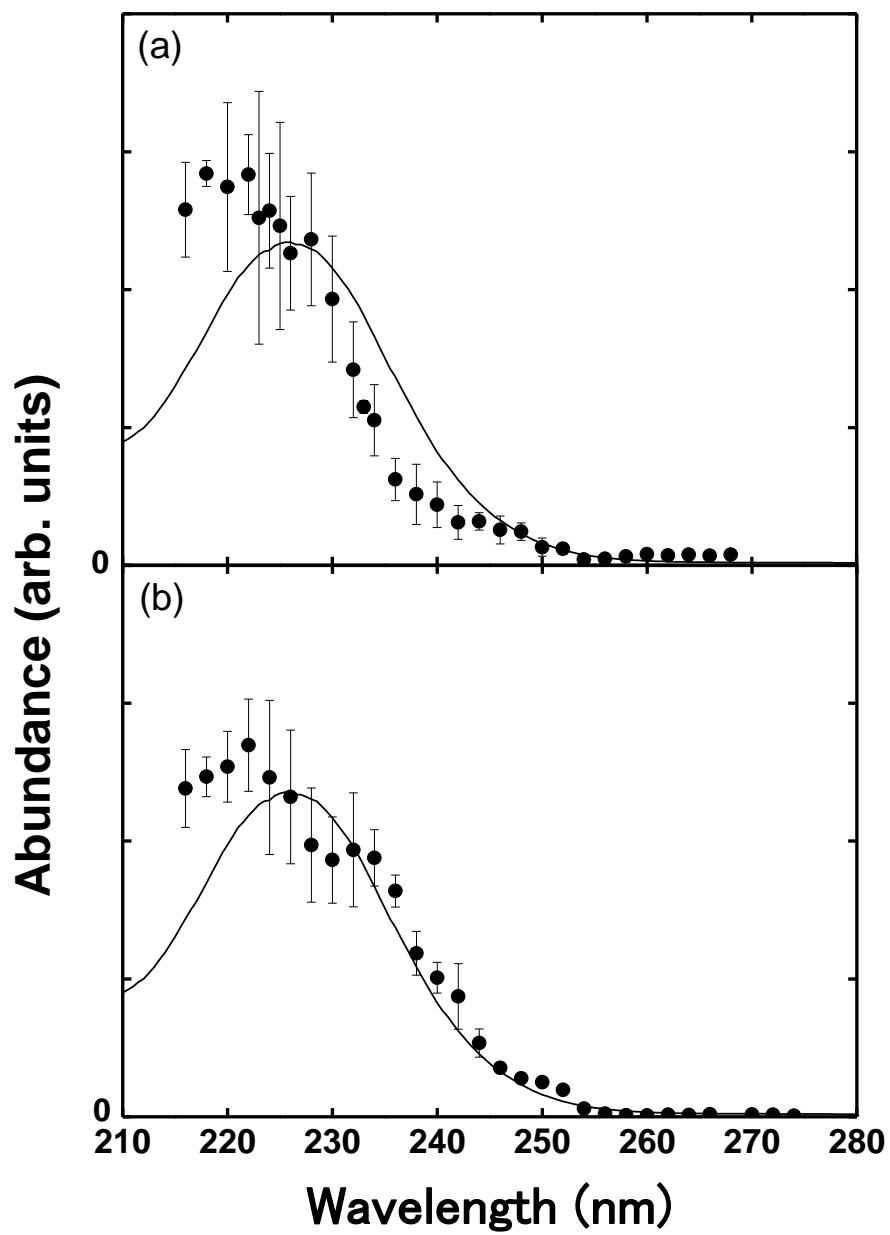


Figure 3.5: Action spectra which represent the total abundances of the cations as a function of the wavelength of the excitation laser for (a) 0.5 and (b) 1.5 M NaI aqueous solution.

3.2.2 Photodetachment from I^- on Aqueous Solution Surface

Sodium iodide, NaI, in water dissociates into an ion-pair, Na^+ and I^- . I^- in water shows characteristic optical absorption in the <250 nm region, the CTTS band. On the other hand, Na^+ in water exhibits optical absorption in the vacuum ultraviolet (VUV) region, since it has a closed-shell electronic structure. Hence, when an aqueous solution of NaI is irradiated with a UV light, which is resonant with the CTTS band (220-250 nm), I^- is electronically excited. As the lifetime of the electronically excited state is 70 ps, the electron near the iodine atom is readily solvated by the surrounding water molecules.^[26]

Neumark and co-workers observed the photoelectron spectrum of solvated electrons ejected from a liquid beam by a nanosecond laser pulse.^[27] They showed that nanosecond laser irradiation of a precursor anion (CN^- or I^-) induces two processes. The first is CTTS excitation of the anion in water followed by the generation of the solvated electron in the liquid beam, and the second is the ejection of the solvated electron into the vacuum. The solvated electrons formed in the earlier part of each laser pulse are able to be further excited within the same laser pulse. As the binding energy of solvated electrons in water is ~ 3.3 eV, the solvated electrons are released from the water by the single photon absorption. The photodetachment processes that occur when I^- in water is irradiated with a nanosecond laser pulse are summarized as follows



where I^{-*} , $e_{(s)}$ and $e_{(free)}$ stand for I^- in the CTTS state, a solvated electron in water, and a free electron in the gas phase, respectively. Thus, the photoelectron spectrum of I^- in water itself is hardly observed when I^- is excited by the nanosecond UV laser pulse.

We recorded the photodetachment spectrum to investigate the electronic structure of I^- in the ground and the excited electronic states.

As shown in Figure 3.1, the pulse energy dependence of the abundance of the electrons is almost linear, although energetics suggests that, at least, the energy that is two times as high as the photon energy is required for the electron ejection from I^- in water. This indicates that one of the reactions (17-19) is the bottleneck process. In addition, the wavelength dependence exhibited in Figure 3.2a is evidently consistent with the CTTS band. Note that the reaction 19 is a bound-free transition showing no clear wavelength dependence. These findings indicate that the reaction 17 is the bottleneck process in the photodetachment processes. Hence, the photodetachment spectrum of I^- is equivalent to the absorption spectrum of I^- .

Because the process 17 is dependent on and the processes 18 and 19 are independent of the I^- concentration, the intensity of the ejected electrons should be linearly proportional to the I^- concentration in the probe region. Note that electron ejection from a deep inside the solution into the gas phase is not possible, and an electron escape depth determines a probe region. Figure 3.3a shows the intensity of electrons ejected into the gas phase as a function of the concentration of NaI in the aqueous solution when the solution was excited at the wavelength of 220 nm. The intensity of the ejected electrons does not change so much with the concentration of NaI. Considering the fact that the I^- concentration in the bulk solution increases linearly with an increase in the NaI concentration, our experimental finding indicates that the electrons are not ejected from the bulk solution but from a surface and just below the surface, and that the I^- concentration in the interfacial region changes differently from the bulk phase with the NaI concentration.

According to the MD simulation, ions in <2 nm below the surface exhibits the specific solvation structure, whereas the region of >2 nm below the surface is regarded as a bulk.^[7-10] Because the electron intensity in the photodetachment spectrum does not change linearly with the concentration of NaI, the electron escape depth is considered to be <2 nm. Our result is consistent with the estimation by Morgner and coworkers, who

measured the photoelectron spectra of liquid-phase molecules excited by either the photoabsorption of He(I) light (UPS) or through collisions with metastable atoms, He* (MIES).^[28] Comparing the spectra, they concluded that the typical probe depth of UPS is 0.5-1 nm, when the kinetic energy of electrons is 10 eV.^[28]

In contrast, there are some reports, where an electron mean free path in water is employed as the electron escape depth. If this is the case, then the electron escape depth is ~30 nm for the electrons having the kinetic energy of 5 eV,^[27] which is inconsistent with our experimental observation. It is likely that there are surface-specific effects that shorten the electron escape depth because the ion concentration is different from the bulk.

3.2.3 Solvation Structure of I⁻ on Aqueous NaI Solution Surface

According to the MD simulation, the region <2 nm from the gas-liquid interface is considered to consist of two layers: a surface and below the surface.^[7-10] Let us discuss the solvation structure of I⁻ in this region based on the photodetachment spectroscopy. As shown in Figure 3.2d, the photodetachment spectrum of I⁻ in the 2.0 M NaI aqueous solution shows another band at longer wavelengths (240 nm). The spectral intensity at 240 nm increases with an increase in the NaI concentration. (See Figure 3.3b.)

Jungwirth and co-workers calculated the difference of binding energies between I⁻ in the bulk solution and surface I⁻, in the ground state and the excited state, respectively.^[8] The result shows that I⁻ in the excited state is stabilized more than I⁻ in the ground state, causing the red shift of the absorption spectrum of I⁻ on the surface. Saykally and his co-workers also mentioned the red shift of the absorption spectrum of I⁻ on the solution surface observed by the second harmonic generation spectroscopy.^[13]

Hence, we assign the peak appearing in the longer wavelength region of the

photodetachment spectra of Figure 3.2 to the CTTS band of I^- on the liquid surface. On the basis of this spectral assignment we conclude that, above a threshold concentration of 0.5 M, I^- ions begin to appear on the surface of the solution and their concentration at the surface then increases as the bulk NaI concentration increases.

In addition, the original band appearing at 220 nm is assignable to the CTTS band of I^- below the surface. It is highly likely that the I^- concentration just below the surface does not change as the bulk NaI concentration increases. The inference is consistent with the MD studies:^[7-10] First, they suggest that halides with large polarizability are able to stay on the aqueous surface because the water molecules arrange themselves around the ion in such a way that they produce a large effective dipole moment.^[10] This large dipole moment polarizes I^- significantly, causing I^- to be stabilized by the large dipole-induced dipole interaction. Second, they suggest that halides with large polarizability are depleted below the surface because I^- is not fully stabilized by the water molecules. In summary, we conclude that I^- locates below the surface only when the concentration is low enough. The I^- ions start to appear on the surface when the NaI concentration is higher than 0.5 M. In contrast, the concentration of I^- ions below the surface does not change with the bulk concentration of NaI.

3.2.4 Solvation Structure of Na^+ on Aqueous Solution Surface Studied by Action Spectrum

When I^- ions in the liquid beam are excited by a UV pulse laser, electrons are ejected from the surface. As a result, the liquid surface becomes positively charged. When the density of the positive charge is high enough, positive ions on the liquid surface are expelled by Coulomb repulsion forces from the surface into the vacuum. Upon ejection, the ions take the neighboring solvent molecules with them, forming cluster ions in the gas phase. We observed these cluster ions using the mass analyzer described in Figure 2.7b. The observed mass spectrum is reported in Figure 3.4. The

spectrum shows a series of ions that are assignable to $\text{Na}^+(\text{H}_2\text{O})_m$ ($m = 0, 1, 2, \dots$), suggesting that Na^+ are ejected into the vacuum with accompanying solvent water molecules. The action spectrum of a 0.5 M NaI shown in Figure 3.5a illustrates the abundance of observed cations as a function of excitation laser wavelength. This action spectrum closely matches the photodetachment spectrum of the same solution. This finding indicates that it is the excitation of the CTTS band of I^- below the surface which triggers the ejection of the cation clusters.

However, at 1.5 M the action spectrum shown in Figure 3.5b is different from the photodetachment spectrum. It is evident that the peak that appears in the longer wavelength region of the corresponding photodetachment spectrum is absent from the action spectrum. Recall that the peak at 250 nm observed in the photodetachment spectrum was attributed the excitation of I^- atoms sitting at the surface. The missing peak in the action spectrum therefore reveals information about the solvation structure of Na^+ on the surface. According to the calculation by Jungwirth and co-workers, Na^+ prefers to be below the surface, hardly appearing on the surface.^[8] The action spectrum is therefore strong evidence that Na^+ does not exist on the surface. In contrast, when I^- below the surface is excited by the 220-240 nm laser light, the observed cluster ions abundance increased dramatically, indicating that Na^+ exists on the inside of the solution at depths of at least 2 nm. In summary, our experimental results provide clear support for the theoretical inference that Na^+ tends to be located below the surface and not at the solution surface.

3.2.5 Mass Spectrometric Study of the Solvation Structure of Na^+ on Aqueous Solution Surface

As mentioned previously, I^- on the surface or I^- below the surface can be excited selectively by tuning the wavelength of the laser. Figure 3.6 panels a and b show mass spectra of ions produced by irradiation of a liquid beam of 1.5 M NaI aqueous solution

with a 224 and 260 nm laser pulse, respectively. The ions produced by irradiation with the 224 nm laser pulse were assigned to $\text{Na}^+(\text{NaOH})_n$ ($n = 0, 1, 2, \dots$) and their hydrated ions, $\text{Na}^+(\text{NaOH})_n(\text{H}_2\text{O})_m$ ($n = 0, 1, 2, \dots, m = 1, 2, 3, \dots$). Although the total ion intensities are weak when 260 nm is employed, we are able to assign the ion peaks in this spectrum to the series $\text{Na}^+(\text{H}_2\text{O})_m$ ($m = 0, 1, 2, \dots$) and $\text{Na}^+(\text{NaOH})(\text{H}_2\text{O})_m$ ($m = 0, 1, 2, \dots$).

Comparison between the mass spectra of Figure 3.6a and b shows that a lot of NaOH are released into the gas phase when I^- below the surface is excited. As NaOH does not exist in the solution as prepared, NaOH must be formed by chemical reactions after photoexcitation. Metal cations are known for being effective scavengers of solvated electrons, forming strong reductants as the result. Therefore, it is highly likely that electrons emitted from I^- will transfer to the Na^+ cations forming neutral Na in the solution.^[29] The neutral Na atoms are then expected to react with H_2O to form NaOH and a hydrogen atom in the following way



In addition, the solvated electrons could also attach to H_2O , forming OH^- and H. The NaOH is produced by the combination of OH^- and Na^+ . However, the rate constant of the electron attachment to H_2O is much smaller than that of metal cations.^[29] It is unlikely that NaOH could be produced in the absence of Na^+ , so the production of NaOH is an indication that there are Na^+ ions in the vicinity of I^- within the liquid beam.

The wavelength dependence of ion species observed in the mass spectra is more quantitatively shown in Figure 3.7. Here, we measured the abundance of each cluster ion from the series, $\text{Na}^+(\text{NaOH})_n(\text{H}_2\text{O})_m$ ($n = 0, 1, 2, \dots, m = 0, 1, 2, \dots$), relative to the total ion abundance. Figure 3.7a illustrates the relative abundance of clusters with

varying values of n . The figure shows that NaOH rich clusters are predominantly formed in the shorter wavelength region, their relative abundance gradually decreasing at wavelengths longer than 240 nm. In contrast, the relative abundance of $\text{Na}^+(\text{H}_2\text{O})_m$ clusters starts to increase with wavelength, becoming totally dominant in the longer wavelength region. The average number of Na atoms included in the clusters as a function of the wavelength of the excitation laser is shown in Figure 3.7b. Note that the Na atoms are present as both Na^+ and NaOH in the gas phase clusters. The average number of Na involved in the clusters remains high in the 220-250 nm range, but drops down close to a value of one at wavelengths greater than 250 nm. Evidently, the wavelength dependence of the formation of the Na rich clusters overlaps the absorption band of I^- below the surface. In contrast, the average number is almost one in the wavelength region where surface I^- exhibits the photoabsorption.

In summary, the action spectra of sodium containing clusters show no characteristic surface absorption peak in the longer wavelength region, even for the most concentrated of NaI solutions. In addition, the mass spectrum of the ions produced by excitation of surface I^- does not exhibit ion peaks assignable to Na rich clusters. These findings lead us to conclude that Na^+ atoms are not likely to be found on the surface of the aqueous solution of NaI.

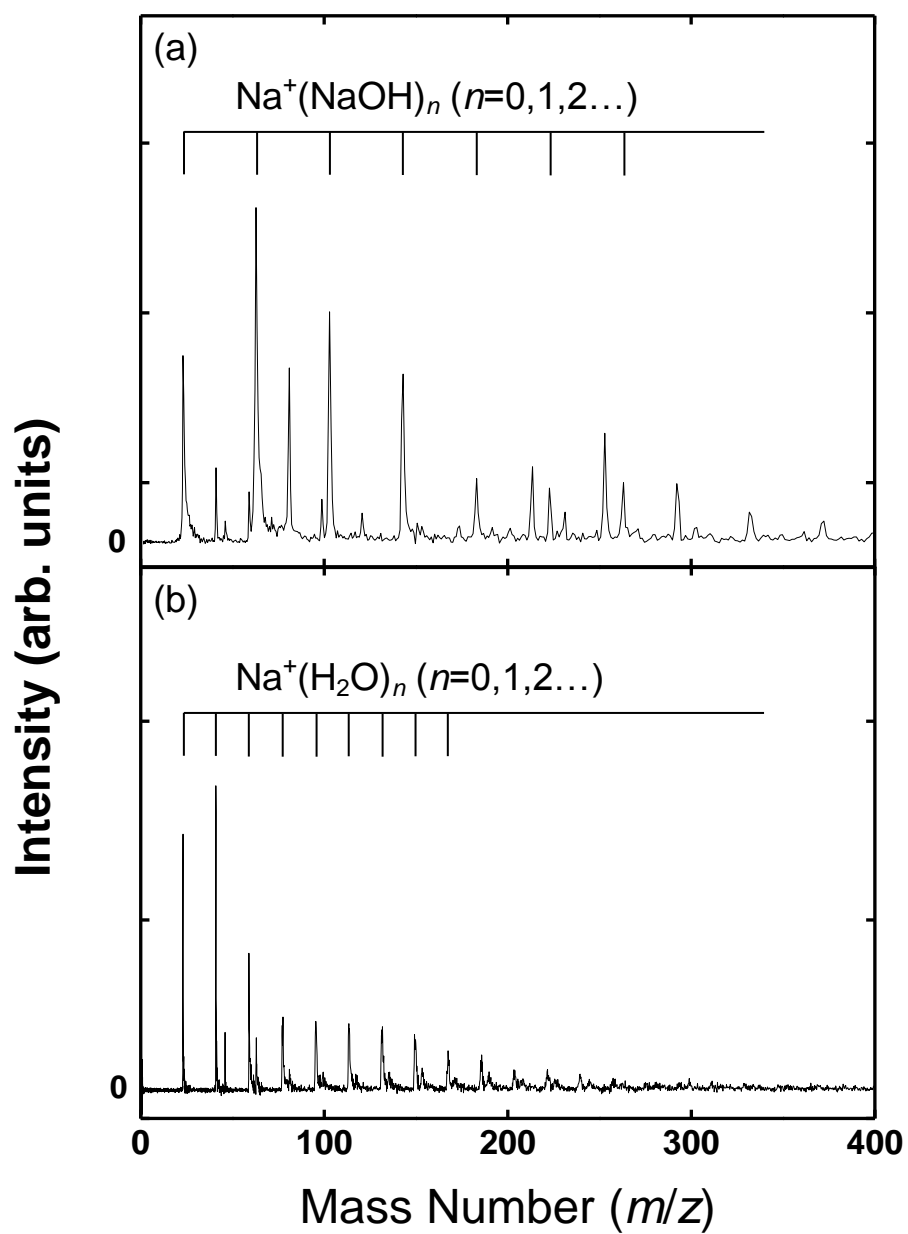


Figure 3.6: TOF mass spectra of the cations produced by irradiation of a (a) 224 and (b) 260 nm laser pulse onto the liquid beam of the 1.5 M NaI aqueous solution.

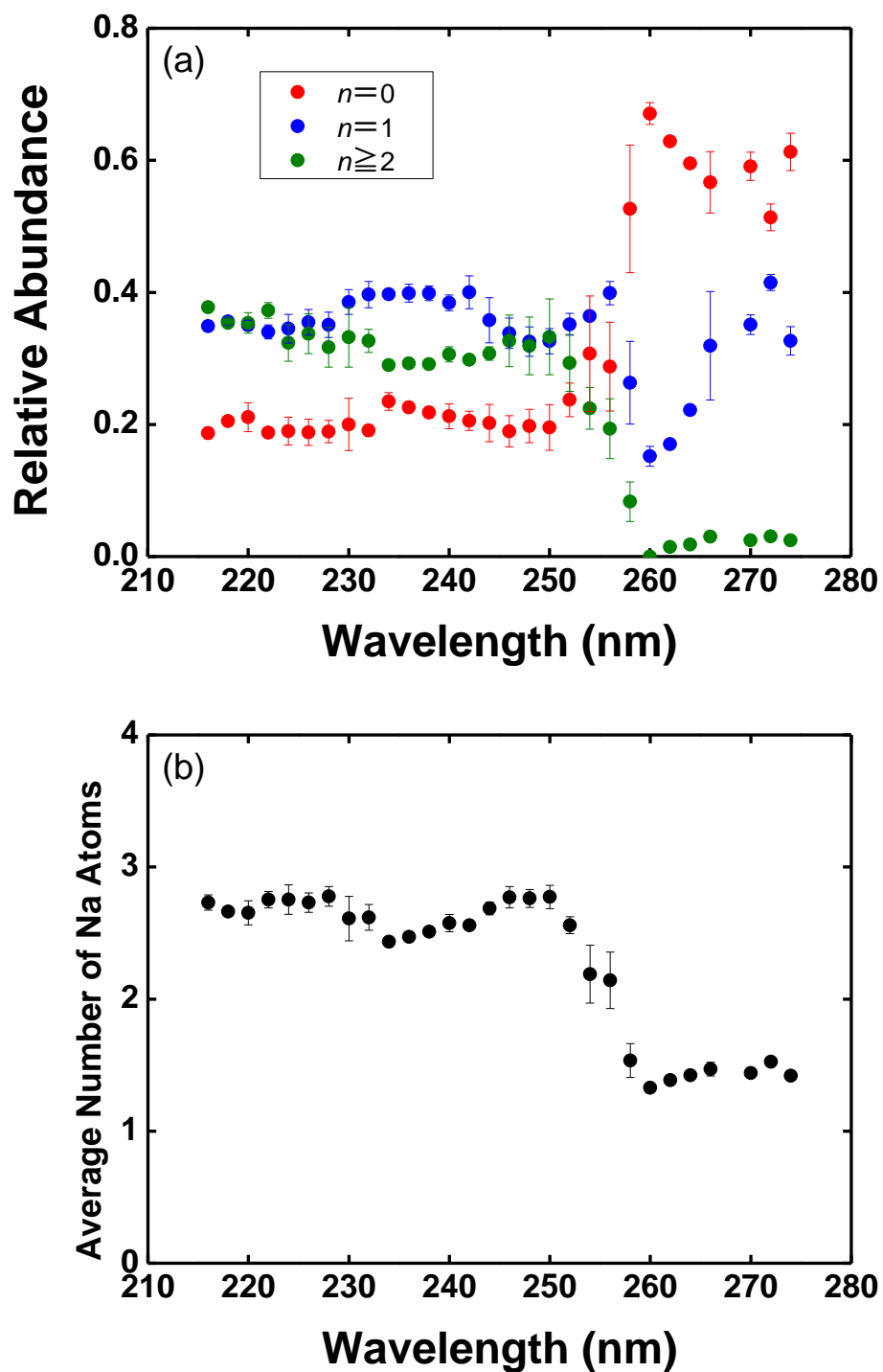


Figure 3.7: (a) The ratio of $\Sigma_m[\text{Na}^+(\text{NaOH})_n(\text{H}_2\text{O})_m]$ ($n = 0, 1, 2, \dots$) for different cluster size, n as a function of the wavelength of the excitation laser. Here, $[X]$ represents the abundance of X . (b) The average number of Na atoms included in the clusters as a function of the wavelength of the excitation laser.

Chapter 4

Solvation Structure of I^- on a Surface of a Mixture Solution of KI and NaCl

4.1 Introduction

In this study, we investigated the effect of the other species on the solvation structure of I^- on a surface by photodetachment spectroscopy. From the measurement of the photodetachment spectrum for a KI aqueous solution, we found the difference of the degree how much I^- is attracted between Na^+ and K^+ . We also measured the photodetachment spectroscopy for a dilute solution of I^- mixed with NaCl. As a result, we elucidated the effect of the less polarizable ions on the solvation structure of the more polarizable ions on the surface.

4.2 Results and Discussion

4.2.1 Solvation Structure of I^- on Aqueous KI Solution Surface

To elucidate the effect of cations on the solvation structure of I^- , we measured the photodetachment spectrum for a KI aqueous solution. Figure 4.1a,b shows the spectra for the 0.5 and 2.0 M KI solution. The spectrum for the 0.5 M KI solution resembles

closely the photoabsorption spectrum of I^- (CTTS band) in an aqueous solution and the photodetachment spectrum of NaI in an aqueous solution as well. (See Figure 3.2a.) This finding indicates that I^- does not stay on the surface when the concentration of KI is low enough (0.5 M). The spectrum for the 2.0 M KI solution resembles the photodetachment spectrum of the 2.0 M NaI solution: There appears the band at longer wavelengths whose spectral intensity is enhanced when the bulk KI concentration is increased to 2.0 M. This finding indicates that I^- appears on the surface when the bulk KI concentration is high. Thus, the surface enhancement of I^- was also observed in the KI solution.

When the photodetachment spectrum for KI was compared with the spectrum for NaI, it was found that the spectral intensity in the longer wavelengths was more enhanced for the NaI solution than for the KI solution. This finding indicates that surface concentration of I^- in the NaI solution is higher than that in the KI solution, even when the prepared bulk concentrations of I^- in the solutions are identical at 2.0 M. The difference in the degree of enhancement of the surface I^- concentration is explained in terms of the interaction between surface I^- and the cations located inside the solution. The cations attract surface I^- inward, lowering the concentration of surface I^- . Hence, the present result suggests that I^- is attracted by K^+ more strongly than by Na^+ . Such interaction was clearly demonstrated by Saykally and his coworkers for HI, NaI, and KI aqueous solutions by SHG measurement.^[30] They found that I^- stays dominantly on the surface in all of the solution, and the concentration of surface I^- is highest for the HI solution. It is because Na^+ and K^+ located inside the solution attract surface I^- inward, whereas H_3O^+ specifically locating on the surface attracts I^- toward the surface.

4.2.2 Enhanced Surface I^- Concentration by Addition of NaCl

As shown in this study, I^- tends to locate below the surface when the concentration is low enough. Then, I^- ions begin to appear on the surface of the solution, and the concentration at the surface increases as the bulk NaI concentration increases. The question to be answered is “where is I^- located when a dilute solution of I^- is mixed with a concentrated solution of Cl^- ?”. It is known that Cl^- tends to be inside the solution because polarizability of Cl^- is too small to be stabilized fully by the water molecules. Figure 4.2 shows photodetachment spectrum of 0.5 M KI solution including 1.5 M NaCl. Comparing the spectrum with that of 0.5 M KI solution (Figure 4.1a), it is evident that another band appears at 240 nm. Note that only I^- is probed in this experiment because there is no photoabsorption band of NaCl in this wavelength range. In fact, no appreciable signals were observed for the pure NaCl aqueous solution in the wavelength range studied. Figure 4.3a,b shows the spectral intensity at 220 and 240 nm, respectively, as a function of the concentration of NaCl. The intensity at 240 nm increases with an increase in the NaCl concentration. The spectral features indicate that I^- located inside the solution is pushed to the surface when NaCl is added to the solution. In contrast, the intensity at 220 nm levels or slightly decreases with the NaCl concentration. The decrease in the signal intensity would suggest that the addition of NaCl expels I^- \sim 2.0 nm below the surface toward the gas-liquid interface. However, it is difficult to see if the decrease is intrinsic.

It is known that I^- on a surface of a liquid droplet reacts with gas-phase O_3 . The reaction rate strongly depends on the concentration of surface I^- . Ammann and his coworkers measured the reaction rate for the liquid droplets containing KI and NaCl at different concentrations.^[31] They found that the reaction rate of a droplet (7.3 M KI) is almost the same as the rate of a droplet (1.0 M KI + 6.3 M NaCl) and hence inferred that the surface I^- concentration of the 7.3 M KI aqueous solution is almost the same as that of the 1.0 M KI + 6.3M NaCl aqueous solution. In the present study, we gave a direct evidence of this inference: Addition of NaCl to the KI solution enhances the

surface concentration of I^- .

As discussed in the previous section, surface concentration of I^- in the NaI solution is higher than that in the KI solution because I^- is attracted inward by K^+ more strongly than by Na^+ . Hence, it is expected that enhancement of the surface I^- concentration by the addition of NaCl is more clearly seen in the NaI solution. Figure 4.4a shows photodetachment spectrum of 0.5 M NaI solution including 0.5 M NaCl. Comparing the spectrum with that of 0.5 M NaI solution (Figure 3.2a), it is evident that another band appears at 250 nm. In addition, the spectral intensity at 250 nm was found to increase with an increase in the NaCl concentration as shown in Figure 4.4b.

Hemminger and his coworkers observed the solvation structure of Br^- at the surface of the NaCl solution doped with Br^- by ambient pressure X-ray photoelectron spectroscopy.^[32] They also showed that more polarizable Br^- tend to stay on the surface in the presence of the less polarizable Cl^- . Hence, we are able to conclude that enhancement of the more polarizable anions on the surface in the presence of the less polarizable ions in the solution is general propensity.

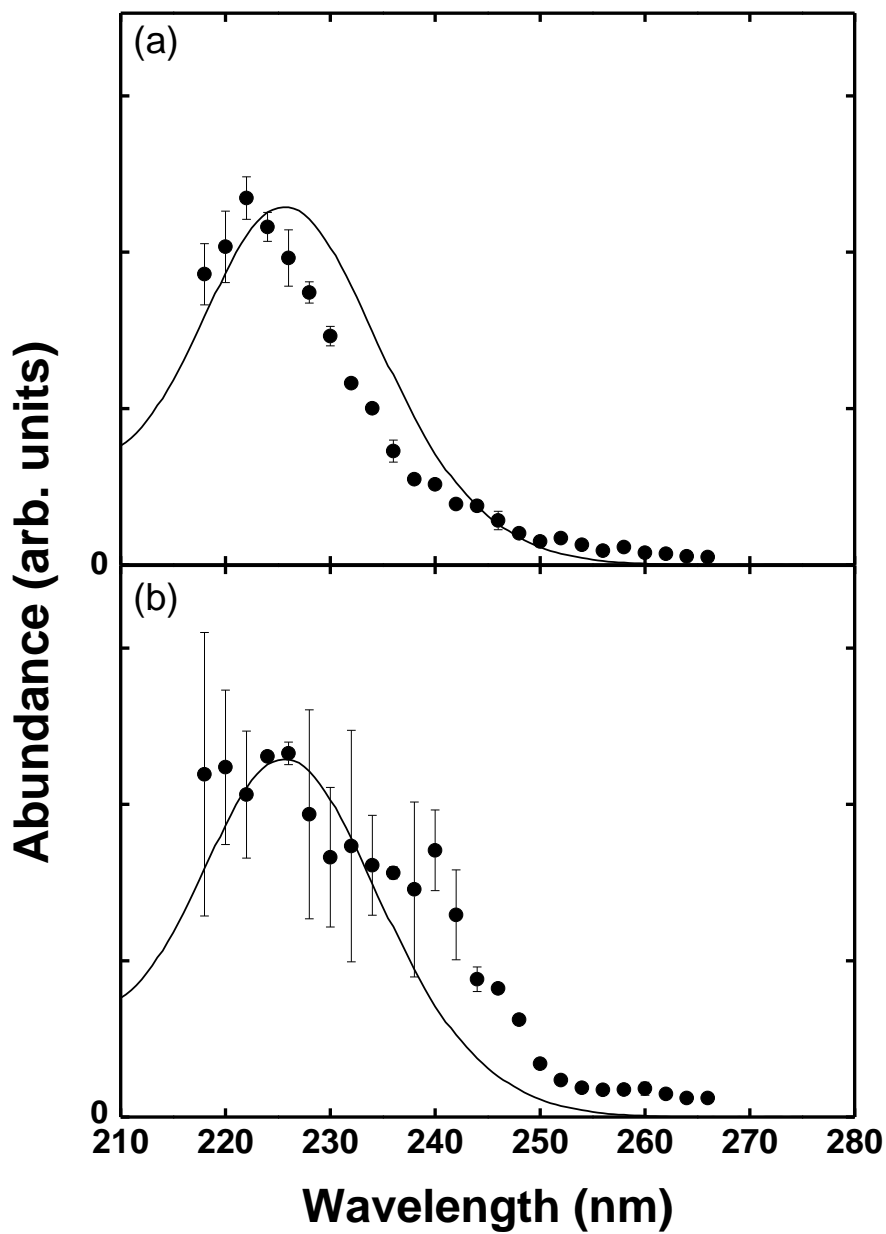


Figure 4.1: Photodetachment spectra for (a) 0.5 M KI aqueous solution and (b) 2.0 M KI aqueous solution. The dashed lines in the Figures represent an absorption spectrum of I^- in an aqueous solution.

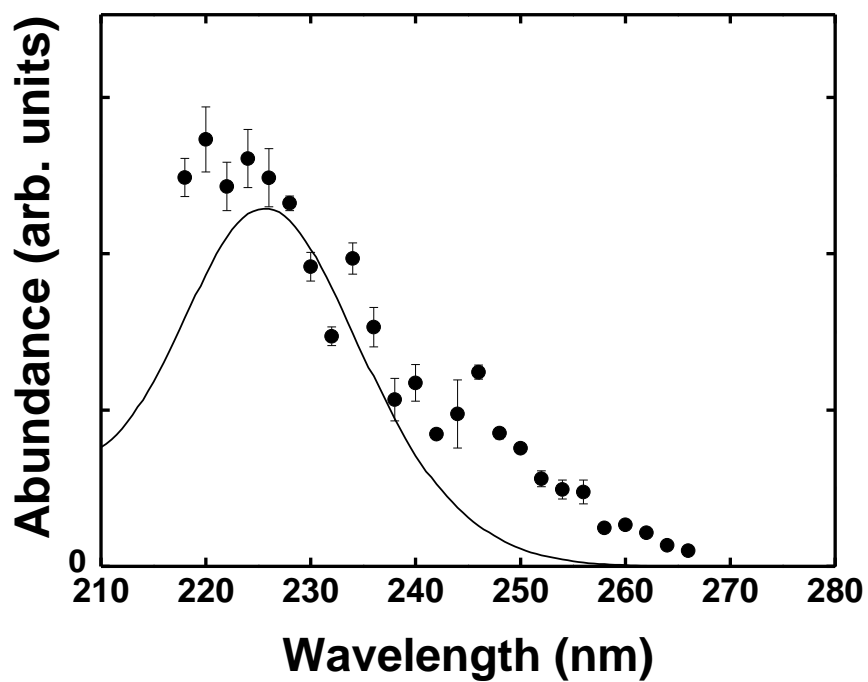


Figure 4.2: Photodetachment spectrum for 0.5 M KI + 1.5 M NaCl aqueous solution. The dashed line in the Figure represents an absorption spectrum of I^- in an aqueous solution.

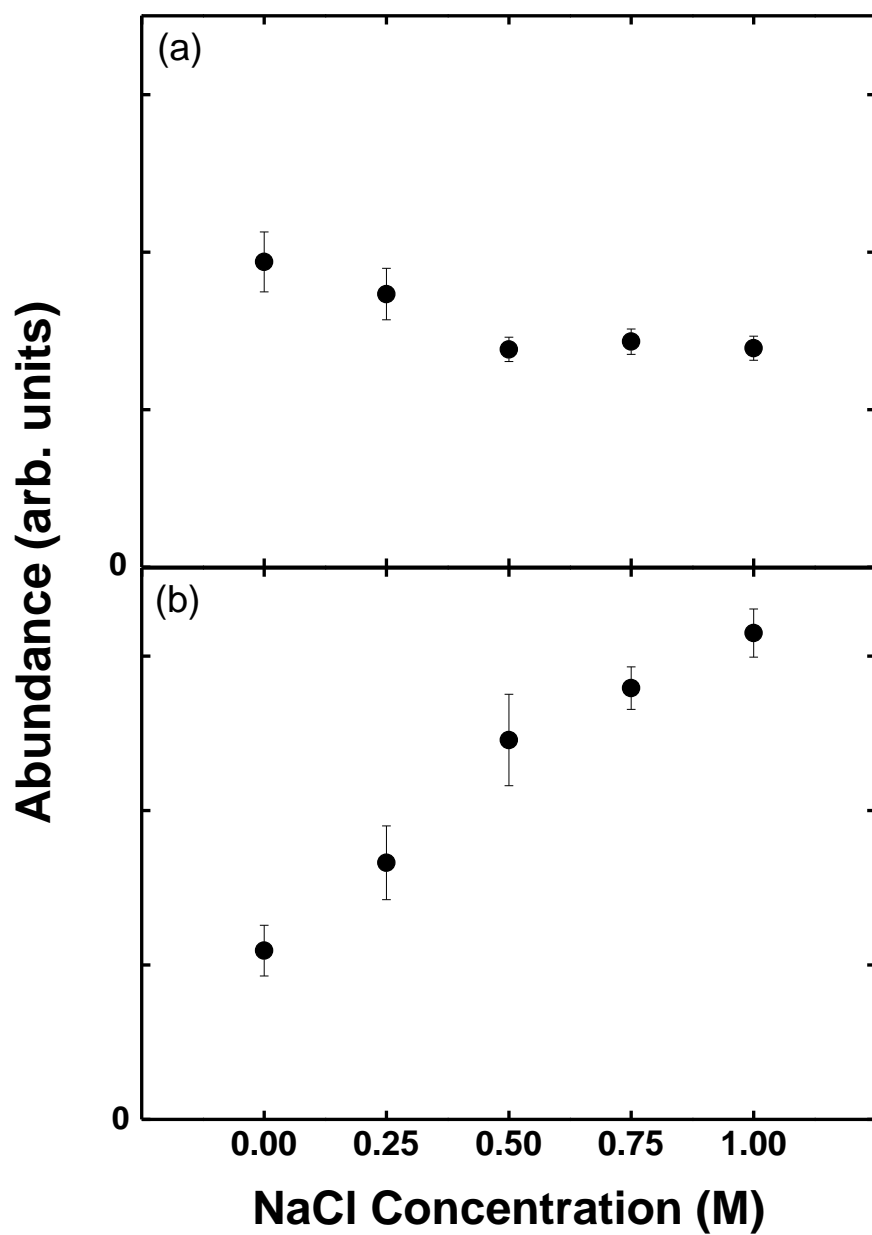


Figure 4.3: Abundance of electrons ejected from the surface of the mixture solution of 0.5 M KI and NaCl as a function of the concentration of NaCl. Panels a and b were obtained when the solution is excited at 220 and 240 nm, respectively.

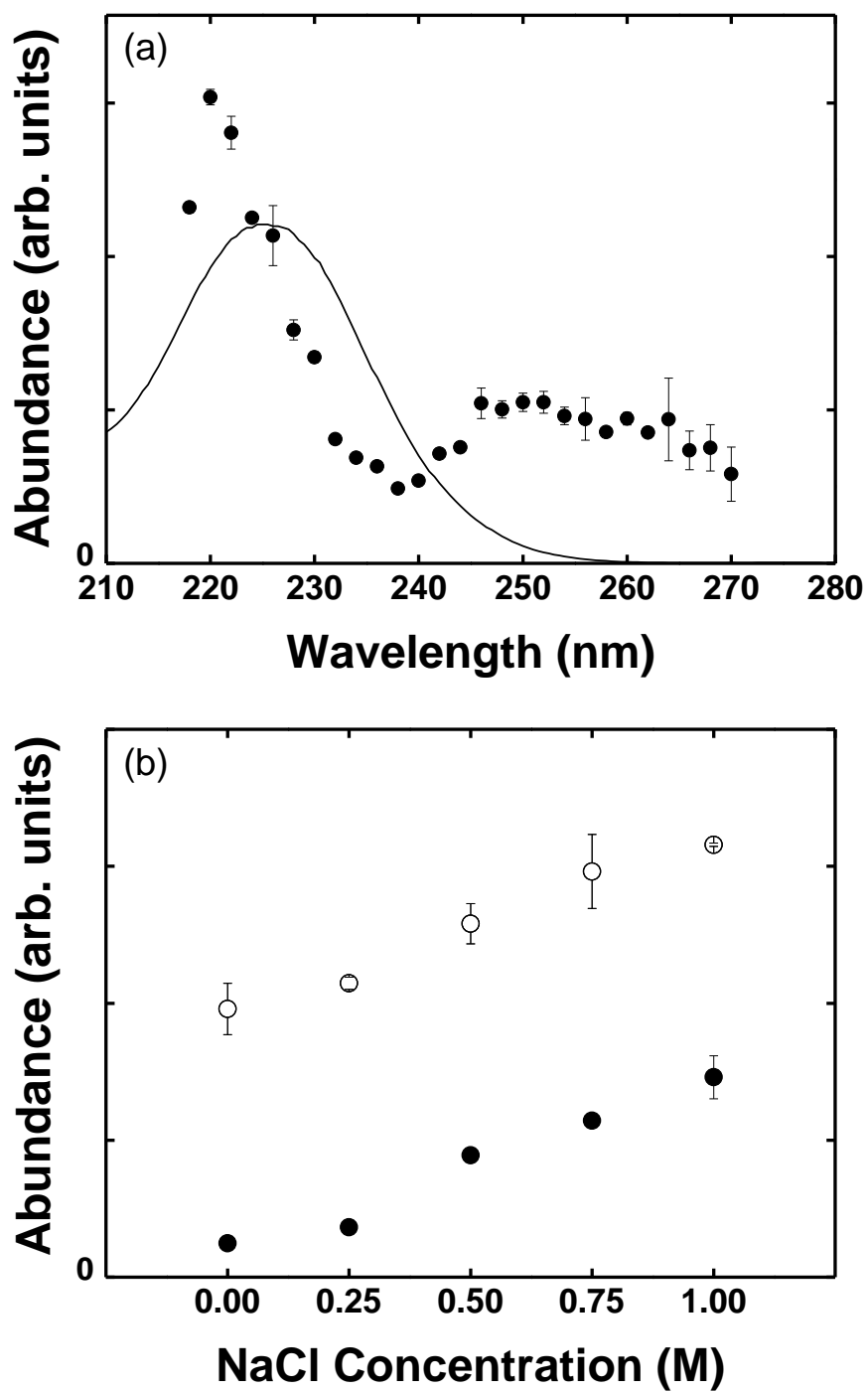


Figure 4.4: (a) Photodetachment spectra for 0.5 M NaI + 0.5 M NaCl aqueous solution. (b) Abundances of electrons ejected from a surface of a mixture solution of 0.5 M NaI and NaCl as a function of the concentration of NaCl. Open and solid circles represent the intensities excited at 220 and 250 nm, respectively.

Chapter 5

Conclusion

We investigated solvation structures of I^- and Na^+ on a NaI aqueous solution surface using a liquid beam by photodetachment spectroscopy and TOF mass spectrometry. We measured photodetachment spectra and action spectra of aqueous solutions of NaI, and obtained the following results.

The photodetachment spectrum of the 1.5 M NaI solution shows a broad peak in the longer wavelength region (>250 nm) which is assignable to surface I^- , whereas the photodetachment spectrum of the 0.5 M solution does not. This difference indicates that I^- is able to exist on the surface when the concentration of NaI is high enough (>1.0 M). On the other hand, neither the action spectrum of cations released from the 0.5 M nor the 1.5 M NaI solution shows any characteristic peak in the longer wavelength region. In addition, although the mass spectra for the 0.5 and 1.5 M NaI solution exhibit Na rich clusters when I^- below the surface was excited, no Na rich clusters were formed by the excitation of surface I^- . These findings lead us to conclude that Na^+ does not exist on the surface of an aqueous solution of NaI.

We also measured the photodetachment spectrum of the KI solution and the mixture solution of KI and NaCl. Similar concentration dependence as the NaI solution was observed for the KI solution. We also found that I^- located inside the solution is pushed to the surface when NaCl is added to the solution. These changes are explained by the difference in the polarizability of halide ions.

As described above, the present technique has high selectivity in that I^- on the surface or I^- below the surface can be selected by scanning the wavelength of the

incident laser. This provided the information about solvation structures of cations, which are hardly determined in the previous research. Furthermore, the liquid beam technique is one of the highly sensitive methods of measurements in combination with photodetachment spectroscopy and mass spectrometry. It is found that our technique is very effective tool that has high sensitivity and selectivity for dealing with liquid surface.

However, there is no doubt that the research probing the liquid surface is very difficult. Many more effective tools probing the liquid surface will be needed.

References

- [1] Heydweiller, A. *Ann. Phys.* **1910**, 33, 145.
- [2] Wagner, C. *Phys. Z.* **1924**, 25, 474.
- [3] Onsager, L.; Samaras, N.N.T. *J. Chem. Phys.* **1934**, 2, 528.
- [4] Weissenborn, P. K.; Pugh, R. J. *J. Colloid Interface Sci.* **1996**, 184, 550.
- [5] Hu, J.H.; Shi, Q.; Davidovits, P.; Worsnop, D.R.; Zahniser, M.S.; Kolb, C.E. *J. Phys. Chem.* **1995**, 99, 8768.
- [6] Knipping, E.M.; Lakin, M.J.; Foster, K.L.; Jungwirth, P.; Tobias, D.J.; Gerber, R.B.; Dabdub, D.; Finlayson-Pitts, B.J. *Science* **2000**, 288, 301.
- [7] Jungwirth, P.; Tobias, D.J. *J. Phys. Chem. B* **2000**, 104, 7702.
- [8] Jungwirth, P.; Tobias, D.J. *J. Phys. Chem. B* **2001**, 105, 10468.
- [9] Jungwirth, P.; Tobias, D.J. *J. Phys. Chem. B* **2002**, 106, 6361.
- [10] Vrbka, L.; Mucha, M.; Minofar, B.; Jungwirth, P.; Brown, E.C.; Tobias, D.J. *Curr. Opin. Coll. Inter. Sci.* **2004**, 9, 67.
- [11] Miranda, P. B.; Shen, Y. R. *J. Phys. Chem. B* **1999**, 103, 3292.
- [12] Liu, D.; Ma, G.; Levering, L.M.; Allen, H.C. *J. Phys. Chem. B* **2004**, 108, 2252.
- [13] Raymond, E.A.; Richmond, G.L.; *J. Phys. Chem. B* **2004**, 108, 5051.
- [14] Petersen, P.B.; Johnson, J.C.; Knutsen, K.P.; Saykally, R.J. *Chem. Phys. Lett.* **2004**, 397, 46.

- [15] Petersen, P.B.; Saykally, R.J.; Mucha, M.; Jungwirth, P. *J. Phys. Chem. B* **2005**, *109*, 10915.
- [16] Petersen, P.B.; Saykally, R.J. *J. Phys. Chem. B* **2006**, *110*, 14060.
- [17] Weber, R.; Winter, B.; Schmidt, P. M.; Widdra, W.; Hertel, I. V.; Dittmar, M.; Faubel, M.; *J. Phys. Chem. B* **2004**, *108*, 4729.
- [18] Ghosal, S.; Hemminger, J.C.; Bluhm, H.; Mun, B.S.; Hebenstreit, E.L.D.; Ketteler, G.; Ogletree, D.F.; Requejo, F.G.; Salmeron, M. *Science* **2005**, *307*, 563.
- [19] Ogletree, D.F.; Bluhm, H.; Lebedev, G.; Fadley, C.S.; Hussain, Z.; Salmeron, M. *Rev. Sci. Instrum.* **2002**, *73*, 3872.
- [20] Faubel, M.; Kisters, Th. *Nature*. **1989**, *39*, 527
- [21] Faubel, M.; Schlemmer, S.; Toennies, J.P. *Z. Phys. D.* **1988**, *10*, 269
- [22] Mafun'e, F.; Takeda, Y.; Nagata, T.; Kondow, T. *Chem. Phys. Lett.* **1992**, *199*, 615
- [23] Parker SP, ed. 1983. *McGraw-Hill Encyclopedia of Physics*. New York: McGraw-Hill
- [24] Blandamer, M.J.; Fox, M.F. *Chem. Rev.* **1970**, *70*, 59
- [25] Kohno, J.; Mafune, F.; Kondow, T. *J. Phys. Chem. A* **2000**, *104*, 243
- [26] Kloepfer, J.A.; Vilchiz, V.H.; Lenchenkov, V.A.; Germaine, A.C.; Bradforth, S.E. *J. Chem. Phys.* **2000**, *113*, 6288.
- [27] Shreve, A.T.; Yen, T.A.; Neumark, D.M. *Chem. Phys. Lett.* **2010**, *493*, 216.

[28] Morgner, H. Low Energy Electrons for the Investigation of Liquid Surfaces. In *Linking the Gaseous and Condensed Phases of Matter: The Behavior of Slow Electrons*; NATO Advanced Study Institute, 1993; pp 92-94.

[29] Buxton, G. V. Radiation Chemistry of the Liquid State: (1) Water and Homogeneous Aqueous Solutions. In *Radiation Chemistry Principles and Applications*; Farhataziz and Rodgers, M. A. J., Eds.; VCH Publishers: New York, 1987; pp 321-349.

[30] Petersen, P.B.; Saykally, R.J. *J. Phys. Chem. B* **2005**, *109*, 7976.

[31] Rouviere, A.; Sosedova, Y.; Ammann, M. *J. Phys. Chem. A* **2010**, *114*, 7085.

[32] Ghosal, S.; Brown, M. A.; Bluhm, H.; Krisch, M. J.; Salmeron, M.; Jungwirth, P.; Heminger, J. C. *J. Phys. Chem. A* **2008**, *112*, 12378.

Appendix

Ionization of Gold Nanoparticles in Solution by Pulse Laser Excitation as Studied by Mass Spectrometric Detection of Gold Cluster Ions

1. Introduction

An optical absorption spectrum of a gold nanoparticle in a solution exhibits a surface plasmon band around 520 nm on a broad interband transition from the visible to the ultraviolet region.^[1-4] A peak profile of the surface plasmon band strongly depends on a diameter of the particle. For the particle whose diameter is smaller than the electron mean free path (~25 nm for gold), the width of the surface plasmon peak increases, whereas the height decreases with a decrease in the particle diameter (>5 nm). On the other hand, the spectral feature of the interband does not change significantly with the diameter of the particle, because it relates to the response of the d electrons.^[1-4]

It is known that a colloidal gold nanoparticle in an aqueous solution is multiply ionized when excited by a nanosecond laser pulse in the wavelength regions of the surface plasmon band and the interband transition.^[5] As the ionization potential of the particle (5.1 eV) is higher than the one-photon energy of the laser pulse, more than two photons should be involved in the ionization process.^[6] However, it is also known that sequential two-photon absorption is not possible, because the lifetime of the excited states is very short.^[7] The ionization mechanism of the metallic nanoparticles is an issue

for intensive investigation.

In our previous study, we obtained a nanosecond transient absorption spectrum of the solution, right after the gold nanoparticles in the solution were excited by a second or third harmonic of the Nd:YAG laser pulse at 532 and 355 nm.^[8] The 532 and 355 nm laser pulses are mainly resonant to the surface plasmon band and the interband transition, respectively. In both cases, the transient absorption spectrum exhibited a broad absorption in the near-IR to the visible region, which was assigned to the solvated electrons. We measured the abundance of the solvated electrons, finding that the ionization yield by the excitation of the interband transition is much higher than that of the surface plasmon band.

To investigate the ionization mechanism, we need to measure the ionization yield as a function of the wavelength in the UV-vis range. However, transient absorption spectroscopy is not highly sensitive enough to measure the ionization yield in the wide wavelength range. Hence, we must increase the pulse energy of the excitation laser as high as ~50 mJ to obtain a reliable transient absorption spectrum of solvated electrons. However, when the aqueous solution is irradiated with the UV laser pulse at 50 mJ, the water molecules are also ionized by multiphoton absorption, and hence, we cannot observe the electrons from the gold nanoparticles exclusively. Actually, we observed intense signals of the solvated electrons, which are independent of the concentration of the gold nanoparticles, when the solution is irradiated with the 266 nm laser pulse.

In the present study, we observed gold ions formed upon ionization of the colloidal gold nanoparticles in the solution. It is known that the ions formed in the vicinity of the solution surface are ejected into the gas phase, which can be detected by mass spectrometry.^[9] The liquid beam is the interface between the solution phase and the gas phase. As the mass spectrometry is highly sensitive, we can reduce the pulse energy of the excitation laser as low as 100 μ J, which prevents multiphoton ionization of the water molecules. In addition, if the water molecules are ionized, we can measure the signals of the gold ions selectively by mass spectrometry. The high sensitivity and the selectivity

of the mass spectrometry allow us to measure the abundance of the gold ions as a function of the wavelength of the excitation laser pulse.

2. Experimental Section

The stock solution of the gold nanoparticles were prepared by laser ablation of a gold metal plate in a sodium dodecyl sulfate (SDS) aqueous solution.^[10-19] Here, the metal plate was placed on a bottom of a glass vessel filled with 10 mL of a 1×10^{-4} M SDS aqueous solution. The fundamental (1064 nm) of a nanosecond Nd:YAG pulsed laser operating at 10 Hz with the pulse energy of 90 mJ was focused by a lens having a focal nanoparticles was 11.0 nm, and the standard deviation of the size distribution was 5.0 nm. The concentration of the particles was typically 1.5 mM after the 36000 laser shots in terms of gold atoms. Hereafter, when the concentration of the nanoparticles is given in this paper, it refers to the concentration of atoms dispersed as particles. When we need to change the concentration of SDS in the solution, we mixed the stock solution of the gold nanoparticles with an SDS aqueous solution.

The gold nanoparticles in the SDS aqueous solution were introduced into a vacuum as a continuous liquid flow (liquid beam). Figure 1 shows a schematic diagram of the experimental apparatus used in the present study, which consists of the liquid beam, a vis-UV nanosecond pulsed laser, and a reflectron time-of-flight (TOF) mass spectrometer. The liquid beam was introduced downward into a vacuum chamber through an aperture with the diameter of 20 μm . The liquid was pressurized at 20 atm by a Shimadzu LC-10Ai pump designed for liquid chromatography, and the flow rate was maintained at 0.2 mL/min. The liquid beam was trapped on a surface of a cryopump cooled by liquid N₂ at 10 cm downstream from the aperture. The chamber was further evacuated down to 10^{-6} - 10^{-7} Torr by a 2400 L/s diffusion pump. Traveling a distance of 1 mm from the aperture, the liquid beam was crossed with the vis-UV laser beam at the first acceleration region of the TOF mass spectrometer. The vis-UV laser is

resonant with the interband transition and/or the surface plasmon band of the gold nanoparticles so that the particles in the liquid beam are excited selectively. The visible laser beam (400-600 nm) was generated by a Quanta-ray PDL-3 dye laser excited by a Quanta-ray GCR-170 Nd:YAG laser. The UV laser beam (200-300 nm) was obtained by frequency-doubling the output of the dye laser using BBO crystals. The pulse output energy was monitored by Coherent FieldMax-P laser energy meter, which was kept at 100-300 μJ . The vis-UV laser was focused onto the liquid beam by an optical lens with a focal length of 300 mm. The beam waist of the excited laser at the interacting region with the liquid beam is about 0.1 mm, which is larger than the diameter of the liquid beam (20 μm).^[20]

Ions ejected from the liquid beam into a vacuum were accelerated by a pulsed electric field in the first and second acceleration region of the TOF mass spectrometer, in the direction perpendicular to both the liquid and the laser beams. The ions were then steered and focused by a set of vertical and horizontal deflectors and an einzel lens. After traveling in a 1 m field-free region, the ions were reversed by the reflectron tilted by 3° off the beam axis and were detected by a Hamamatsu microchannel plate. Signals from the multiplier were amplified by a homemade 100 MHz preamplifier and processed by a Tektronics TDS 500A digital oscilloscope. The mass resolution, $m/\Delta m$, was more than 100 at $m = 200$ in the present experimental condition.

3. Results

Figure 2 shows a mass spectrum of ions produced by irradiation of a 440 nm laser pulse onto the liquid beam of the gold nanoparticles in a 0.05 M SDS aqueous solution. Peaks assignable to gold cluster ions, Au_n^+ ($n = 1, 2, 3, \dots$), and their hydrated ions, $\text{Au}_n^+(\text{H}_2\text{O})_m$ ($n = 1, 2, 3, \dots, m = 1, 2, 3, \dots$) lying at the heavy side from respective Au_n^+ peaks, are seen in the mass spectrum. In addition, there are a series of cluster ions, $\text{Na}^+(\text{H}_2\text{O})_n$, in the lower mass region. These ions originate from Na^+ which is dissolved

in the aqueous solution as a cation of SDS. When we increased either the pulse energy of the laser or the concentration of gold nanoparticles, no remarkable changes were observed in the cluster size distribution.

Now, let us focus on the abundance of the gold ions, $\Sigma_m \Sigma_n [\text{Au}_m^+(\text{H}_2\text{O})_n]$ ($m \geq 1, n \geq 0$), where [] stands for the abundance of the ion of interest. Figure 3 shows the abundance as a function of the concentration of the gold nanoparticles: it increases almost linearly with an increase in the concentration. Figure 4a illustrates the abundance as a function of the SDS concentration in an aqueous solution. The abundance was almost zero when the SDS concentration is lower than 10^{-4} M. The abundance increases gradually with an increase in the SDS concentration. Then, it increases drastically at the critical micelle concentration (cmc) of SDS (8.3 mM), and levels off above it. The abundance of solvated electrons measured in our previous study is also shown in Figure 4a, which depends on the SDS concentration similarly with the abundance of the gold ions. The question to be answered here is why the ionization yield is highest above the cmc of SDS. In an aqueous solution, SDS dissociates into Na^+ and DS^- , and DS^- forms micelles above the cmc, which interact strongly with the nanoparticles. It is known that the negative charge of the micelles is able to stabilize electrostatically the hole formed upon ionization.^[21] This partial charge neutralization results in a decrease in the ionization potential and, hence, increases the ionization yield.^[21]

Figure 4b shows the relations between the abundance of the solvated electrons and that of the ions obtained from the data in Figure 4a. The abundance of the ions is always proportional to that of the solvated electrons. Figure 5 shows the abundance of gold ions as a function of the wavelength of the excitation laser. As the optical absorption spectrum of gold nanoparticles exhibits a characteristic surface plasmon band at 520 nm on a broad interband transition extending from the visible to the UV region, the abundance could change with the wavelength accordingly. However, the abundance decreases monotonically as the wavelength increases. This finding indicates that the photoionization of the gold nanoparticles is not caused by the resonant enhanced multiphoton ionization.

4. Discussion

Ionization and Ion Ejection from the Liquid Beam. Gold nanoparticles in an aqueous SDS solution are ionized when irradiated with a nanosecond laser pulse in the UV-vis region. Here, electrons are released from the particles into the solution, and positively charged particles are formed simultaneously. The emitted electrons are solvated readily by water, turning into solvated electrons.^[22-24] In fact, we observed the solvated electrons which were formed right after the pulse laser irradiation, by the nanosecond transient absorption spectroscopy.^[8] Figure 4a shows the abundance of solvated electrons as a function of the concentration of SDS. It increases gradually with an increase in the SDS concentration and drastically at the cmc of SDS. We calculated the number density of solvated electrons according to the Lambert-Beer law and estimated the charge states of the gold nanoparticles.^[5] It was found that the particles are so multiply charged that they become unstable, because the Coulomb repulsive forces exceed the cohesive forces operating inside each particle, causing fragmentation of the gold nanoparticles due to the Coulomb explosion.^[25-27]

In the present study, we observed the gold cluster ions in the gas phase by mass spectrometry (see Figure 2). This finding indicates that the gold cluster ions are further ejected from the liquid beam surface into the vacuum as a result of the Coulomb explosion of the multiply charged cluster ions. As the size distribution of the cluster ion in the mass spectra does not change appreciably with the concentration of the nanoparticles in the solution, it is highly likely that each particle behaves independently upon fragmentation without the interaction between the nanoparticles.

In addition, it is highly likely that only the small cluster ions are ejected into the gas phase from the liquid beam surface. In fact, we were not able to observe larger cluster ions in the gas phase using an Even cup which allows us to detect the larger ones by the post acceleration of ions at 10 kV. The nascent larger cluster ions once ejected into the gas phase could dissociate by the excitation laser pulse in the gas phase, as the excitation laser pulse illuminates outside of the liquid beam. However, we can rule out

this possibility, because the cluster size distribution did not change appreciably when we increased the pulse energy of the laser beam: the possibility of the photodissociation should increase with an increase in the pulse energy.

In this relation, we must emphasize the fact that the abundance of the cluster ions is proportional to the abundance of the solvated electrons, as is shown in Figure 4b. Hence, we are able to estimate the ionization yield of the gold nanoparticles by observing the cluster ions ejected into the gas phase.

Thermionic Emission by Cyclic Photoexcitation-Relaxation. As discussed above, gold nanoparticles are multiply ionized when irradiated with a nanosecond laser pulse in the UV-vis region. As the abundance of the gas-phase cluster ions is proportional to the abundance of the electrons, the action spectrum of the cluster ions in Figure 5 should provide the ionization yield of the nanoparticles as a function of the excitation wavelength. Obviously, the action spectrum is different from the absorption spectrum: there is no peak corresponding to the surface plasmon band at 520 nm in the action spectrum.

It is well-known that excited gold nanoparticles are swiftly relaxed to the ground state in picosecond time scale through the strong electron-electron and electron-phonon couplings.^[28-30] Then, the nanoparticles are ready to absorb another photon in the nanosecond laser pulse, which are excited again. The particles are excited repeatedly through this photoexcitation-relaxation cycle, because the absorption cross section of them is large enough^[31] and the photon density of the excitation laser pulse is high enough.^[8] The photon energy absorbed by the particles in each cycle is converted to heat, causing the temperature of them to rise. It follows that the gold nanoparticles are ionized by the thermionic emission.^[8] In fact, theoretical calculation for the 2.6 nm gold nanoparticles suggests that more than 90% of the conduction electrons can be released from them by the thermionic emission when illuminated by the 0.5 ns laser pulse (351 nm, 0.3 J/cm²).^[7]

El-Sayed and co-workers studied the ultrafast optical response of the surface plasmon band of gold nanoparticles.^[28,29] They found the optical bleach of the band when the nanoparticles are excited by the laser pulse at 600 nm. The photoexcitation of the intraband leads to the heating of the conduction electron gas, creating an equilibrium hot electron distribution around the Fermi level. The redistribution of electrons give rise to the optical bleach around 550 nm, which recovers biexponentially with lifetimes of 2.5 and >50 ps. On the other hand, Gu et al. studied the optical response of the interband transition when the nanoparticles are excited by the laser pulse at 305 nm.^[30] They observed a transient absorption at 400 nm, which decays biexponentially through a fast electron-phonon interaction (2 ps) and a slow phonon-phonon interaction (>15 ps). In summary, the transient absorption in the 500-550 nm region is depleted when the intraband is excited, whereas the transient absorption in the UV region is increased when the interband is excited.

The optical bleaching implies that the gold nanoparticles are not ready to absorb a photon within the period after the photoexcitation. Hence, this effect decelerates the photoexcitation-relaxation cycles, which reduces the ionization yield of the particles as much as the surface plasmon band can be disregarded in the excitation processes. The action spectrum in Figure 5 clearly indicates that the photoexcitation-relaxation cycles proceed when the gold nanoparticles are irradiated with the nanosecond laser pulse.

5. Conclusion

Gold nanoparticles in an aqueous SDS solution were multiply ionized when irradiated with a nanosecond laser pulse in the UV-vis region. We observed both the electrons released from the gold nanoparticles by the nanosecond transient absorption spectroscopy and fragment ions ejected into the vacuum by mass spectrometry in combination with the liquid beam technique. The abundance of the ions was measured as a function of the wavelength of the excitation laser (action spectrum). The action spectrum exhibited no peak corresponding to the surface plasmon band at 520 nm,

agreeing well with the component of the interband transition in the absorption spectrum. This finding indicates that the gold nanoparticles were multiply ionized by the thermionic emission, after they are thermally excited by the repetitive photoexcitation-relaxation cycles.

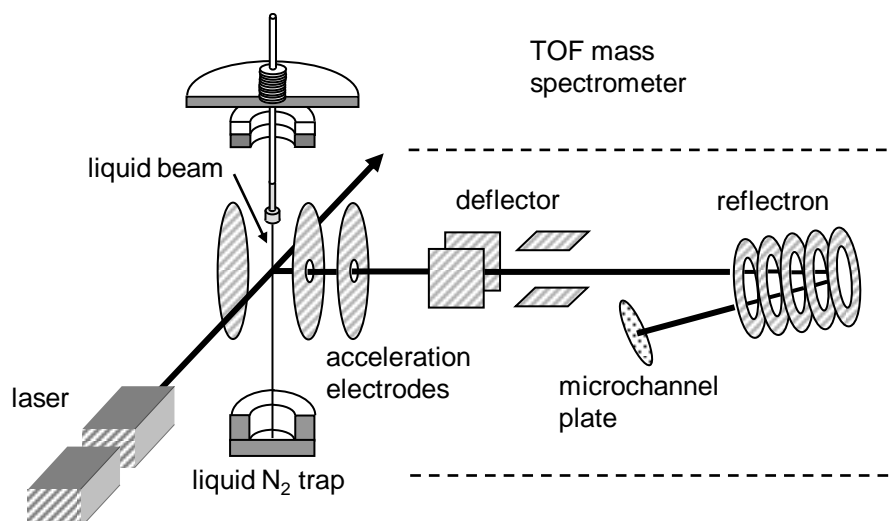


Figure 1. Schematic diagram of a liquid beam source and a TOF mass spectrometer.

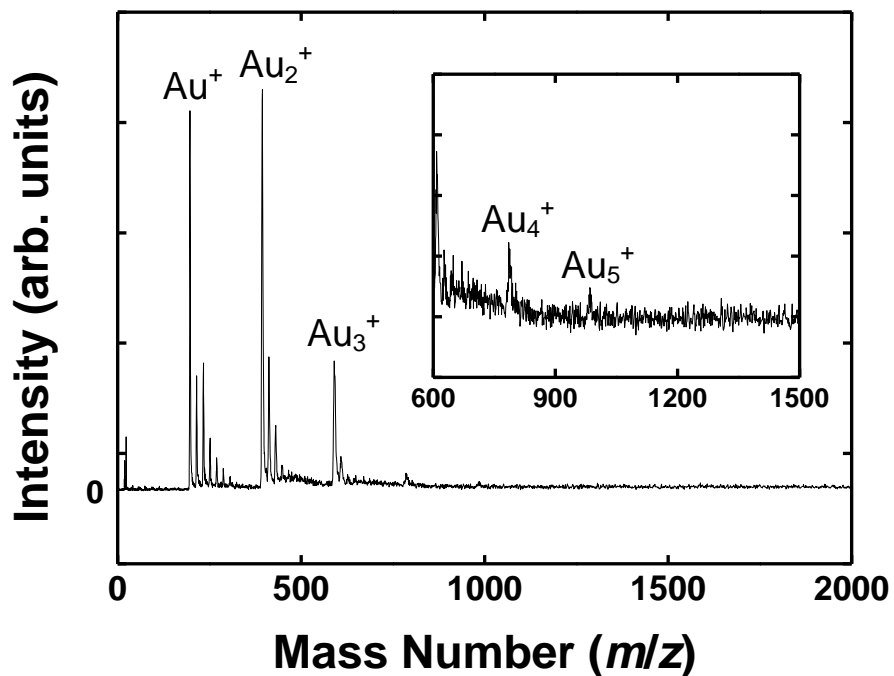


Figure 2. TOF mass spectrum of ions produced by irradiation of a 440 nm laser pulse onto the liquid beam of a 0.05 M SDS aqueous solution containing 2 mM gold nanoparticles.

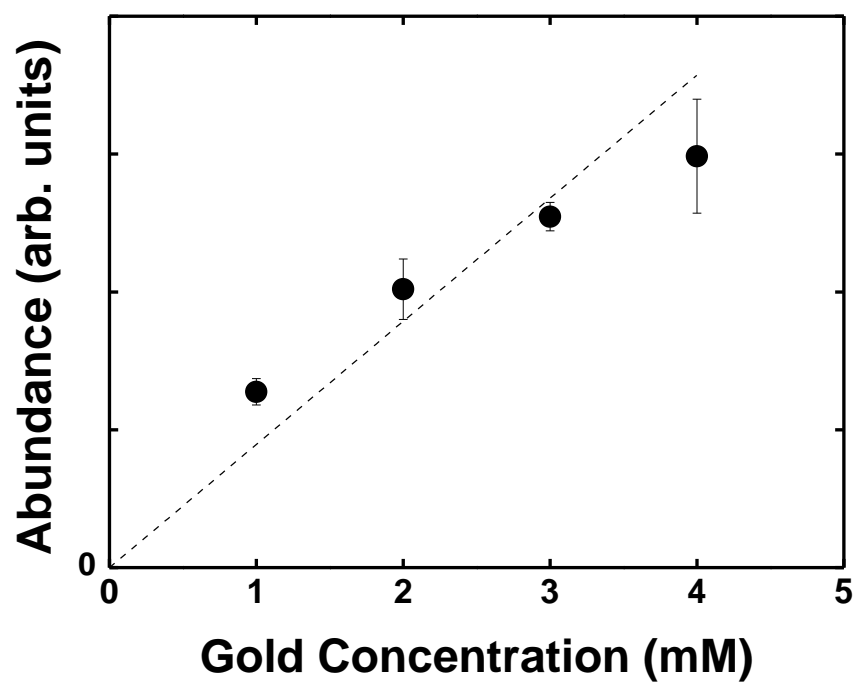


Figure 3. Total abundance of $[\text{Au}_n(\text{H}_2\text{O})_m]^+$ as a function of the concentration of the gold in a 0.05 M SDS aqueous solutions.

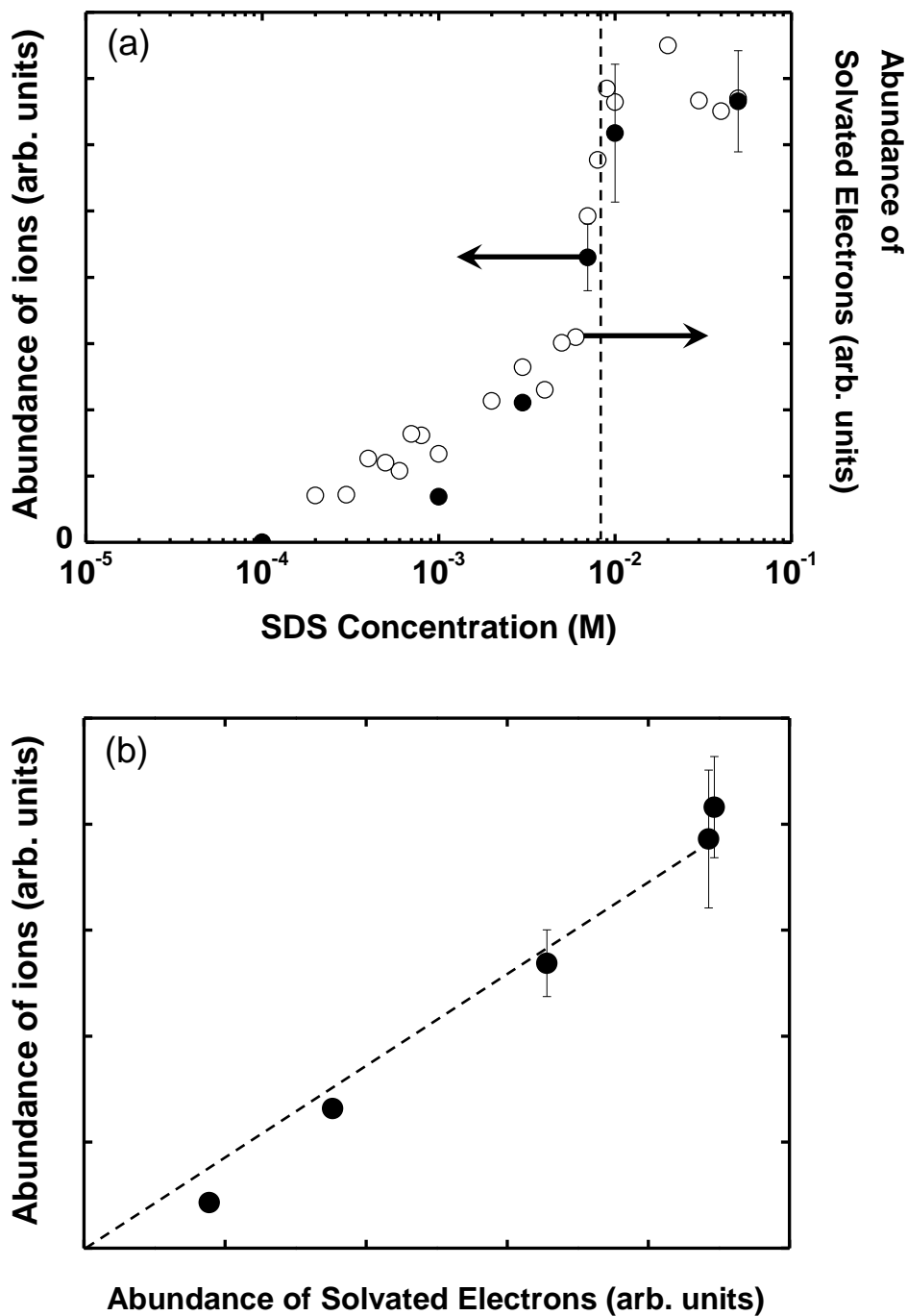


Figure 4. (a) Total abundance of $[\text{Au}_n(\text{H}_2\text{O})_m]^+$ as a function of the concentration of SDS in an aqueous solution containing 1 mM gold nanoparticles (solid circles). The abundance of solvated electrons measured by transient absorption spectroscopy in our previous study is also shown by the open circles. The dash line represents the position of the cmc of SDS (8.3 mM). (b) The relation between the abundance of the solvated electrons and the abundance of the gas-phase cluster ions obtained from panel (a).

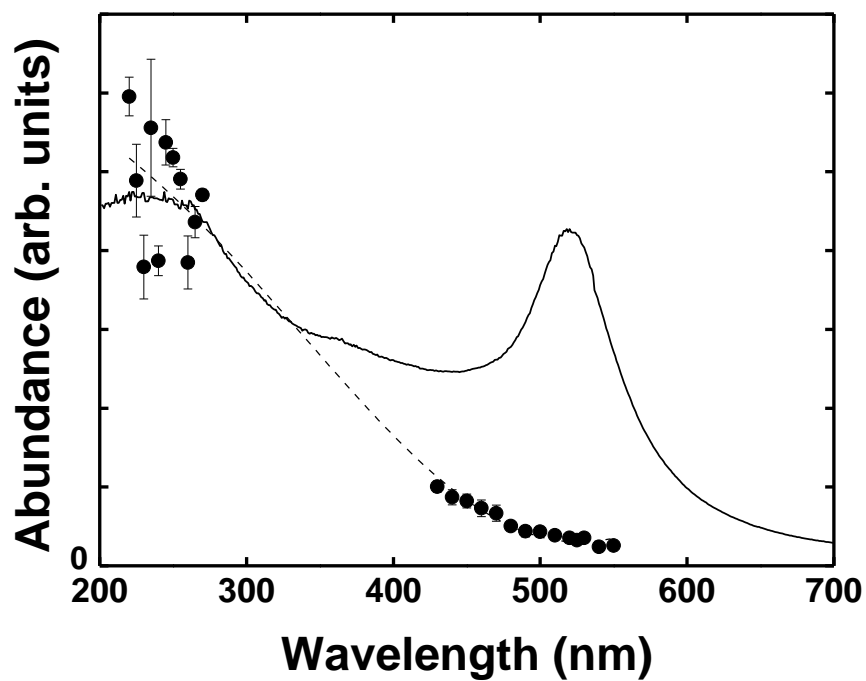


Figure 5. Total abundance of $[\text{Au}_n(\text{H}_2\text{O})_m]^+$ as a function of the wavelength of the excitation laser in a 0.05 M SDS aqueous solution containing 2 mM gold nanoparticles (solid circles) and the optical absorption spectrum of a gold nanoparticle in a solution (solid line). The dash line shows the eye a guide for the action spectrum.

References and Notes

- [1] Bohren, C. F.; Huffman, D. R. *Absorption and Scattering of Light by Small Particles*; Wiley: New York, 1983.
- [2] Doremus, R. H. *J. Chem. Phys.* **1964**, *40*, 2389.
- [3] Kreibig, U.; Frangstein, C. v. *Z. Phys.* **1969**, *224*, 307.
- [4] Kreibig, U. *J. Phys. F: Met. Phys.* **1974**, *4*, 999.
- [5] Yamada, K.; Tokumoto, Y.; Nagata, T.; Mafune', F. *J. Phys. Chem. B* **2006**, *110*, 11751.
- [6] *CRC Handbook of Chemistry and Physics*, 74th ed.; Lide, D. R., Ed.; CRC Press: London, 1993.
- [7] Grua, P.; Marreeuw, J. P.; Bercegol, H.; Jonusauskas, G.; Valle'e, F. *Phys. ReV. B* **2003**, *68*, 035424.
- [8] Yamada, K.; Miyajima, K.; Mafune', F. *J. Phys. Chem. B* **2007**, *111*, 11246.
- [9] Kondow, T.; Mafune', F. *Annu. ReV. Phys. Chem.* **2000**, *51*, 731.
- [10] Sibbald, M. S.; Chumanov, G.; Cotton, T. M. *J. Phys. Chem.* **1996**, *100*, 4672.
- [11] Yeh, M. S.; Yang, Y. S.; Lee, Y. P.; Lee, H. F.; Yeh, Y. H.; Yeh, C. S. *J. Phys. Chem. B* **1999**, *103*, 6851.
- [12] Mafune', F.; Kohno, J.; Takeda, Y.; Kondow, T.; Sawabe, H. *J. Phys. Chem. B* **2000**, *104*, 8333.
- [13] Mafune', F.; Kohno, J.; Takeda, Y.; Kondow, T.; Sawabe, H. *J. Phys. Chem. B* **2000**, *105*, 5114.

- [14] Tsuji, T.; Iryo, K.; Watanabe, N.; Tsuji, M. *Appl. Surf. Sci.* **2002**, *202*, 80.
- [15] Watanabe, N.; Kawamata, J.; Toshima, N. *Chem. Lett.* **2004**, *33*, 1368.
- [16] Usui, H.; Sasaki, T.; Koshizaki, N. *Chem. Lett.* **2006**, *35*, 752.
- [17] Li, M.; Lu, Q.; Wang, Z. *Int. J. Nanosci.* **2006**, *5*, 259.
- [18] Zeng, H.; Cai, W.; Li, W.; Hu, J.; Liu, P. *J. Phys. Chem. B* **2005**, *109*, 18260.
- [19] Sylvestre, J.-P.; Poulin, S.; Kabashin, A. V.; Sacher, E.; Meunier, M.; Luong, J. H. T. *J. Phys. Chem. B* **2004**, *108*, 16864.
- [20] Horimoto, N.; Kohno, J.; Mafune, F.; Kondow, T. *Chem. Phys. Lett.* **2000**, *318*, 536.
- [21] Naik, D. B.; Schnabel, W. *Chem. Phys. Lett.* **1999**, *315*, 416.
- [22] Marbach, W.; Asaad, A. N.; Krebs, P. *J. Phys. Chem. A* **1999**, *103*, 28.
- [23] Jou, F.-Y.; Freeman, G. R. *J. Phys. Chem.* **1979**, *83*, 2382.
- [24] Ayotte, P.; Johnson, M. A. *J. Chem. Phys.* **1997**, *106*, 811.
- [25] Na'her, U.; Bjørnholm, S.; Frauendorf, S.; Garcias, F.; Guet, C. *Phys. Rep.* **1997**, *285*, 245.
- [26] Saunders, W. A. *Phys. ReV. A* **1992**, *11*, 46.
- [27] Manil, B.; Ntamack, G. E.; Lebius, H.; Huber, B. A.; Duft, D.; Leisner, T.; Chandezon, F.; Guet, C. *Nucl. Instrum. Methods Phys. Res., Sect. B* **2003**, *205*, 684.
- [28] Logunov, S. L.; Ahmadi, T. S.; El-Sayed, M. A.; Khoury, J. T.; Whetten, R. L. *J. Phys. Chem. B* **1997**, *101*, 3713.

[29] Jain, P. K.; Qian, W.; El-Sayed, M. A. *J. Phys. Chem. B* **2006**, *110*, 136.

[30] Gu, T.; Ye, T.; Simon, J. D.; Whitesell, J. K.; Fox, M. A. *J. Phys. Chem. B* **2003**, *107*, 1765.

[31] Jain, P. K.; Lee, K. S.; El-Sayed, I. H.; El-Sayed, M. A. *J. Phys. Chem. B* **2006**, *110*, 7238.

Acknowledgements

The present thesis is the summary of my studies from 2004 to 2008 at the Graduate School of Arts and Sciences, University of Tokyo, under the guidance of Professor Fumitaka Mafune. I cordially thanks Professor Fumitaka Mafune for his kind guidance, and creating the best environment for study.

Acknowledgement is also made to members of Mafune Laboratory; Dr. Ken Miyajima, Yujiro Hiranuma, Keisuke Kaniwa, Naoya Fukushima, Hitomi Muto, Natsumi Matsuo, Takehiro Kato, Kunihiro Yamada and Yuki Tokumoto.

I am also grateful to Dr. Kenta Odagiri, Dr. Mauo Sogo, Dr. Takashi Yoshikawa, Yuichi Sakamoto, Olivia Maselli and Fong Yuen Yan. They are my best friends.

Finally, I wish to express my gratitude to my family and my friends for their encouragement and support.

Tokyo, Japan, March 2012

Makoto Shoji